

THE SPATIAL HOMOGENEITY OF NEBULAR AND STELLAR OXYGEN ABUNDANCES IN THE LOCAL GROUP DWARF IRREGULAR GALAXY NGC 6822¹

HENRY LEE², EVAN D. SKILLMAN², AND KIM A. VENN^{2,3}

Full version with color figures at <http://www.astro.umn.edu/~hlee>

ABSTRACT

To test the existence of a possible radial gradient in oxygen abundances within the Local Group dwarf irregular galaxy NGC 6822, we have obtained optical spectra of 19 nebulae with the EFOSC2 spectrograph on the 3.6-m telescope at ESO La Silla. The extent of the measured nebulae spans galactocentric radii in the range between 0.05 kpc and 2 kpc (over four exponential scale lengths). In five H II regions (Hubble I, Hubble V, K α , K β , KD 28e), the temperature-sensitive [O III] λ 4363 emission line was detected, and direct oxygen abundances were derived. Oxygen abundances for the remaining H II regions were derived using bright-line methods. The oxygen abundances for three A-type supergiant stars are slightly higher than nebular values at comparable radii. Linear least-square fits to various subsets of abundance data were obtained. When all of the measured nebulae are included, no clear signature is found for an abundance gradient. A fit to only newly observed H II regions with [O III] λ 4363 detections yields an oxygen abundance gradient of -0.14 ± 0.07 dex kpc⁻¹. The gradient becomes slightly more significant (-0.16 ± 0.05 dex kpc⁻¹) when three additional H II regions with [O III] λ 4363 measurements from the literature are added. Assuming no abundance gradient, we derive a mean nebular oxygen abundance $12+\log(\text{O}/\text{H}) = 8.11 \pm 0.10$ from [O III] λ 4363 detections in the five H II regions from our present data; this mean value corresponds to $[\text{O}/\text{H}] = -0.55$.

Subject headings: galaxies: abundances — galaxies: dwarf — galaxies: evolution — galaxies: individual (NGC 6822) — galaxies: irregular

1. INTRODUCTION

The evolution of element abundances with time provides important clues to the history of chemical enrichment and star formation in galaxies. Abundances in H II regions provide information about the most recent period of metals enrichment in the interstellar medium, now illuminated by recently-formed O, B-type stars. Dwarf irregular galaxies contain few metals and are thought to be chemically homogeneous. These low-mass, metals-poor, gas-rich, and star-forming systems provide unique venues to examine detailed processes of star formation within environments which may be related to star-forming systems observed at early times. Thus far, no nearby ($D \approx 5$ Mpc) dwarf irregular galaxy has ever exhibited a significant radial abundance gradient (i.e., Kobulnicky & Skillman 1996, 1997; Lee & Skillman 2004; Lee et al. 2005). A possible reason is that the most recent burst of star formation has expelled the most recent synthesis of metals into the hot phase of the interstellar medium, and that these metals have yet to cool and “rain” back down onto the cooler phases of the interstellar medium (e.g., Tenorio-Tagle 1996; Kobulnicky & Skillman 1997). It would indeed be very interesting to find an example of a dwarf galaxy with localized oxygen enrichment. Recent developments in high-efficiency spectrographs on 8- and 10-m telescopes have made possible spectroscopy of bright blue A-type supergiants in nearby dwarf irregular galaxies (e.g., Venn et al. 2003; Kaufer et al. 2004). These young hot massive stars allow for the simultaneous measurements of present-day α - and iron-group elements. These measurements also allow for the direct comparison of stellar α -

element abundances with nebular measurements, as massive stars and nebulae are similar in age and have similar formation sites.

NGC 6822 is the nearest gas-rich dwarf irregular galaxy in the Local Group (Mateo 1998). Basic properties are listed in Table 1; see also van den Bergh (2000). Studies of the stellar populations and the star formation history of NGC 6822 are described by Gallart et al. (1996a,b,c), Cohen & Blakeslee (1998), Hutchings et al. (1999), Tolstoy et al. (2001), Wyder (2001), and Clementini et al. (2003). A large H I halo extending much farther out than the optical extent was discovered by Roberts (1972), and confirmed by de Blok & Walter (2000) and Komiyama et al. (2003). A population of young, blue stars was found, whose spatial distribution is farther than the accepted optical radius and is very similar to that of the H I extent (Battinelli et al. 2003; de Blok & Walter 2003; Komiyama et al. 2003). With the characterization of the spatial and color-magnitude distributions of red giant and asymptotic giant branch stars across the entire galaxy in the near-infrared, Cioni & Habing (2005) found a metallicity spread of 1.56 dex from the ratio of carbon- to M-type stars. Leisy et al. (2005) have recently reported 13 new candidate planetary nebulae (PNe), bringing to 17 total PNe in all. Muschiello et al. (1999) obtained spectra of three B-type supergiant stars, and reported a mean iron abundance of $[\text{Fe}/\text{H}] = -0.5 \pm 0.2$. Venn et al. (2001) reported for the first time oxygen abundances for two A-type supergiant stars in NGC 6822, and showed that the mean stellar oxygen abundance was higher than the known H II region nebular abundances by at least 0.1 dex. Because their stars were at low galactocentric radii, the authors suggested the possibility of a radial gradient in oxygen abundance.

The recent measurements of oxygen abundances in A-type supergiant stars have motivated the reevaluation of pub-

¹ Based on EFOSC2 observations collected at the European Southern Observatory, Chile: proposal #71.B-0549(A).

² Department of Astronomy, University of Minnesota, 116 Church St. SE, Minneapolis, MN 55455; hlee@astro.umn.edu, skillman@astro.umn.edu

³ Department of Physics & Astronomy, Macalester College, 1600 Grand Avenue, Saint Paul, MN 55105; venn@macalester.edu

⁴ We use the notation: $[\text{X}/\text{Y}] = \log(\text{X}/\text{Y}) - \log(\text{X}/\text{Y})_{\odot}$.

lished nebular oxygen abundances in NGC 6822. Spectra of and abundances for the brightest H II regions in NGC 6822 were reported by Peimbert & Spinrad (1970), Alloin (1974)⁵, Smith (1975), Lequeux et al. (1979), Talent (1980), and Pagel et al. (1980). However, all of these spectra were obtained with inherently nonlinear detectors, and in many cases the character of the nonlinearities were not understood until well after publication (e.g., Jenkins 1987); so, subsequent corrections for nonlinearity were not possible. Skillman et al. (1989) obtained CCD spectroscopy to measure [O III] $\lambda 4363$ in Hubble V, and derived an oxygen abundance of $12+\log(\text{O}/\text{H}) = 8.20$. In two planetary nebulae, Richer & McCall (1995) derived oxygen abundances ($12+\log(\text{O}/\text{H}) = 8.01, 8.10$) in agreement with published H II region oxygen abundances. Miller (1996) remeasured Hubble V and Hubble X, and derived oxygen abundances $12+\log(\text{O}/\text{H}) = 8.32$ and 8.36 , respectively. In their program on open clusters, Chandar et al. (2000) also obtained spectra for a few nebulae, and derived smaller nebular oxygen abundances than expected. We have reanalyzed a number of their H II region spectra, which we discuss in Sect. 4. Hidalgo-Gómez et al. (2001) also obtained spectra of Hubble V and Hubble X, and while there were no large differences in oxygen abundances between the two H II regions, they claimed small-scale abundances variations on < 10 pc length scales. Nollenberg et al. (2002) derived sulfur abundances from *ISO* measurements of [S III] and [S IV] emission lines in the mid-infrared, and showed that the S^{+3} ion is the largest contributor to the total sulfur abundance in extragalactic H II regions. With VLT data, Peimbert et al. (2005) derived recombination-line abundances for the H II region Hubble V, and showed that their derived oxygen abundances were in better agreement with the stellar oxygen abundances. Some of these results are discussed further in Sec. 4.2 below.

This is the second of two papers of our study examining the spatial homogeneity of oxygen abundances in Local Group dwarf irregular galaxies; WLM was discussed previously in Lee et al. (2005). The main goal here was to obtain a homogeneous set of nebular spectra for H II regions in NGC 6822 over a large range in galactocentric radii. The outline of this paper is as follows. Descriptions of the observations, reductions, measurements and analysis are presented in Sect. 2. Element abundances and abundance ratios are described in Sect. 3. In Sect. 4, we compare present results with recent studies, and examine the presence of spatial inhomogeneities in oxygen abundances. A summary is given in Sect. 5. For the present discussion, we use the notation $[\text{O}/\text{H}] = \log(\text{O}/\text{H}) - \log(\text{O}/\text{H})_{\odot}$, where the solar value of the oxygen abundance is $12+\log(\text{O}/\text{H}) = 8.66$ (Asplund et al. 2004; Meléndez 2004).

2. OBSERVATIONS AND MEASUREMENTS

2.1. Observations and Reductions

Long-slit spectroscopic observations of nebulae in NGC 6822 were carried out on 2003 Aug. 26–28 and 31 (UT) with the ESO Faint Object Spectrograph and Camera (EFOSC2) instrument on the 3.6-m telescope at ESO La Silla Observatory. “Blue” spectra with a smaller wavelength range and low-dispersion spectra with larger wavelength coverage into the red were obtained with gratings 7 and 11, respectively. Details of the instrumentation employed and the log of observations are listed in Tables 2 and 3,

respectively. Observations were obtained during new moon phase. Two-minute $\text{H}\alpha$ acquisition images were obtained in order to set an optimal position of the slit. Typically, the slit angle was set to obtain spectra for more than one H II region. Average departures of the slit position angle from the parallactic angle are listed in Table 3. Nineteen nebulae for which spectra were obtained are listed in Table 3 and are identified in Figs. 1 to 4. Identifications for the nebulae follow from the $\text{H}\alpha$ imaging by Killen & Dufour (1982) and Hodge et al. (1988), and are matched with the $\text{H}\alpha$ image from the Local Group Survey (Massey et al. 2002)⁶. The well-studied bright H II region Hubble V (e.g., Smith 1975; Talent 1980; Pagel et al. 1980; Skillman et al. 1989; Miller 1996; Hidalgo-Gómez et al. 2001) was also observed to check the reliability of our measurements for oxygen abundances.

Data reductions were carried out in the standard manner using IRAF⁷ routines. Data obtained on a given night were reduced independently. The raw two-dimensional images were trimmed and the bias level was subtracted. Dome flat exposures were used to remove pixel-to-pixel variations in response. Twilight flats were acquired at dusk each night to correct for variations over larger spatial scales. To correct for the “slit function” in the spatial direction, the variation of illumination along the slit was taken into account using dome and twilight flats. Cosmic rays were removed in the addition of multiple exposures for a given H II region. Wavelength calibration was obtained using helium-argon (He-Ar) arc lamp exposures taken throughout each night. Exposures of standard stars Feige 110, G138–31, LTT 1788, LTT 7379, and LTT 9491 were used for flux calibration. The flux accuracy is listed in Table 3. Final one-dimensional spectra for each H II region were obtained via unweighted summed extractions.

2.2. Measurements and Analysis

Emission-line strengths were measured using software developed by M. L. McCall and L. Mundy; see Lee (2001) and Lee et al. (2003b,c). In all, [O III] $\lambda 4363$ was detected in five H II regions; these spectra are shown in Figs. 5 and 6. The corrections for reddening and underlying Balmer absorption are described in Lee & Skillman (2004) and Lee et al. (2005). For nebulae with blue spectra, observed flux (F) and corrected intensity (I) ratios are listed in Tables 4a to 4b inclusive. Flux and intensity ratios for nebulae with low-dispersion spectra are presented in Tables 5a to 5c inclusive. In high signal-to-noise spectra, we derived the logarithmic reddening, $c(\text{H}\beta)$, from the error weighted average of values for $F(\text{H}\alpha)/F(\text{H}\beta)$, $F(\text{H}\gamma)/F(\text{H}\beta)$, and $F(\text{H}\delta)/F(\text{H}\beta)$ ratios, while simultaneously solving for the effects of underlying Balmer absorption with equivalent width, EW_{abs} ; see Fig. 9 for H II region Hubble V. We assumed that EW_{abs} was the same for $\text{H}\alpha$, $\text{H}\beta$, $\text{H}\gamma$, and $\text{H}\delta$. In the data tables, we have included the logarithmic reddening and the equivalent width of the underlying Balmer absorption at $\text{H}\beta$. Where negative values were derived, the reddening was set to zero in correcting line ratios and for abundance calculations.

3. NEBULAR ABUNDANCES

⁶ More about the Local Group Survey is found at <http://www.lowell.edu/users/massey/lgsurvey.html>.

⁷ IRAF is distributed by the National Optical Astronomical Observatories, which are operated by the Associated Universities for Research in Astronomy, Inc., under cooperative agreement with the National Science Foundation.

⁵ Alloin (1974) did not derive an oxygen abundance as their [O III] $\lambda\lambda 4959, 5007$ emission lines were saturated and not measured.

3.1. H II Regions

Oxygen abundances in H II regions were derived using three methods: (1) the direct method (e.g., Dinerstein 1990; Skillman 1998); and the bright-line methods discussed by (2) McGaugh (1991), which is based on photoionization models; and (3) Pilyugin (2000), which is purely empirical. These methods are explained in detail in Lee & Skillman (2004) and Lee et al. (2005); we briefly summarize them here.

3.1.1. Oxygen Abundances: [O III] $\lambda 4363$ Temperatures

The “direct” conversion of emission-line intensities into ionic abundances requires a reliable estimate of the electron temperature of the ionized gas. We adopt a two-zone model for H II regions, with a low- and a high-ionization zone characterized by temperatures $T_e(\text{O}^+)$ and $T_e(\text{O}^{+2})$, respectively. The temperature in the O^{+2} zone is measured with the emission-line ratio $I([\text{O III}] \lambda 5007)/I([\text{O III}] \lambda 4363)$ (Osterbrock 1989). The temperature in the O^+ zone is given by

$$t_e(\text{O}^+) = 0.7 t_e(\text{O}^{+2}) + 0.3, \quad (1)$$

where $t_e = T_e/10^4$ K (Campbell et al. 1986; Garnett 1992). The total oxygen abundance by number is given by $\text{O}/\text{H} = \text{O}^+/\text{H}^+ + \text{O}^{+2}/\text{H}^+$. For conditions found in typical H II regions and those presented here, very little oxygen in neutral form is expected, and in the absence of He II emission, the O^{+3} contribution is considered negligible. For subsequent calculations of ionic abundances, we assume the following electron temperatures for specific ions (Garnett 1992; Thuan et al. 1995): $t_e(\text{N}^+) = t_e(\text{O}^+)$, $t_e(\text{Ne}^{+2}) = t_e(\text{O}^{+2})$, $t_e(\text{Ar}^{+2}) = 0.83 t_e(\text{O}^{+2}) + 0.17$, and $t_e(\text{Ar}^{+3}) = t_e(\text{O}^{+2})$.

Derived ionic and total abundances are listed in Tables 6a and 6b, which include derived O^+ and O^{+2} electron temperatures, O^+ and O^{+2} ionic abundances, and the total oxygen abundances. Direct H II region oxygen abundances were derived for Hubble I, Hubble V, $\text{K}\alpha$, $\text{K}\beta$, and KD 28e, and were in excellent agreement with those derived from the method described by Skillman et al. (2003).

Where [S II] $\lambda\lambda 4068, 4076$ and [O II] $\lambda\lambda 7320, 7330$ were detected in the spectra for Hubble V, $\text{K}\alpha$, and KD 28e, we used the IRAF task `temden` in the STSDAS nebular package (Shaw & Dufour 1995) to derive $T_e(\text{S}^+)$ and $T_e(\text{O}^+)$ from $I([\text{S II}] \lambda\lambda 6716, 6731)/I([\text{S II}] \lambda\lambda 4068, 4076)$ and $I([\text{O II}] \lambda 3727)/I([\text{O II}] \lambda\lambda 7320, 7330)$, respectively. $T_e(\text{S}^+)$ would be too low, if [S II] $\lambda\lambda 4068, 4076$ was faint and barely detected. $T_e(\text{O}^+)$ would be too high, if the [O II] $\lambda\lambda 7320, 7330$ flux was too high, which would arise from second-order contamination at wavelengths below 3700 Å. However, we did not use a second-order blocking filter in our spectroscopy program. Nevertheless, we list these temperatures in Tables 6b and 6c.

Electron densities were derived for H II regions Hubble V, $\text{K}\alpha$, and KD 28e from their low-dispersion spectra. With their computed O^{+2} temperatures, the electron densities are 63, 332, and 123 cm^{-3} , respectively. Derived values for the electron density did not change significantly with an assumed O^{+2} temperature of 10^4 K, or when O^+ temperatures are used in the computations. Also, very little change in oxygen abundances for Hubble V, $\text{K}\alpha$, and KD 28e occurred when an electron density of 100 cm^{-3} was assumed.

3.1.2. Oxygen Abundances: Bright-Line Methods

In H II regions without [O III] $\lambda 4363$ measurements, the bright-line method has been used to derive oxygen abundances, as the latter are given in terms of bright [O II]

and [O III] emission lines, i.e., $R_{23} = [I([\text{O II}] \lambda 3727) + I([\text{O III}] \lambda\lambda 4959, 5007)]/I(\text{H}\beta)$ indicator suggested by Pagel et al. (1979) and discussed by Skillman (1989). McGaugh (1991) developed a grid of photoionization models and suggested using R_{23} and ionization factor, $O_{32} = I([\text{O III}])/I([\text{O II}])$, to estimate the oxygen abundance⁸. To break the degeneracy in the bright-line method, we have used the $I([\text{N II}])/I([\text{O II}])$ ratio (e.g., McCall et al. 1985; McGaugh 1994; van Zee et al. 1998; Lee et al. 2003b) to choose between the “upper branch” (high oxygen abundance) or the “lower branch” (low oxygen abundance). In some instances, oxygen abundances with the McGaugh method could not be computed, because the R_{23} values were outside of the effective range for the models. Pilyugin (2000, Equation 4) proposed an empirical calibration at low metallicity with fits of oxygen abundance against bright oxygen lines. Skillman et al. (2003) have shown that while the Pilyugin calibration covers a larger range in R_{23} , the calibration applies mostly to H II regions with higher ionizations; see also the discussion by van Zee & Haynes (2005).

Oxygen abundances derived using the McGaugh and Pilyugin bright-line calibrations are listed in Tables 6a and 6b. For each H II region, differences between direct and bright-line abundances are shown as a function of O_{32} and R_{23} in Fig. 10. The difference between the McGaugh and Pilyugin calibrations (indicated by asterisks) correlates with $\log O_{32}$, which has been discussed by Skillman et al. (2003), Lee et al. (2003a), and Lee & Skillman (2004). We find that bright-line abundances with the McGaugh and the Pilyugin calibrations are about ± 0.10 dex and up to 0.20 dex larger, respectively, compared to the corresponding direct abundances. Generally, in the absence of [O III] $\lambda 4363$, an estimate of the oxygen abundance from the bright-line calibration is good to within ≈ 0.2 dex.

3.2. Supernova Remnants

The emission-line ratio criterion⁹ $I([\text{S II}] \lambda\lambda 6716, 6731)/I(\text{H}\alpha) \gtrsim 0.4$ has been used to distinguish supernova remnants (SNRs) from photoionized H II regions and planetary nebulae at near-solar metallicities (e.g., D’Odorico et al. 1980; Smith 1975; Smith et al. 1993; Levenson et al. 1995). Skillman (1985) found that strong [O I] emission ($I([\text{O I}])/I(\text{H}\beta) \gtrsim 0.1$) indicates the presence of shocks from supernova remnants; whereas in typical H II regions, there is very little oxygen in the form of neutral oxygen (e.g., Baldwin et al. 1981; Veilleux & Osterbrock 1987; Stasińska 1990). We list examples of oxygen abundances in SNRs within nearby dwarf galaxies. Miller (1995) used the shock models of Dopita et al. (1984) to estimate oxygen abundances for two shock-heated nebula in the M 81 group dwarf galaxy Holmberg IX, and found that the estimated mean oxygen abundance ($12 + \log(\text{O}/\text{H}) \approx 8$) was comparable to other dwarf galaxies at similar total (optical) luminosity. Applying the MAPPINGS code to spectrophotometric data, Russell & Dopita (1990) determined that the mean oxygen abundances for SNRs in the Magellanic Clouds were 0.12 to 0.20 dex lower than the mean oxygen abundances derived for the H II regions. However, the errors associated with the abundance differences were also consistent with zero difference between the SNRs and the H II regions. We should

⁸ Analytical expressions for the McGaugh calibration can be found in Kobulnicky et al. (1999).

⁹ This is hereafter referred as $I([\text{S II}])/I(\text{H}\alpha)$.

note that the line ratios used to determine abundances for supernova remnants have been calibrated to the metallicity of the Milky Way, and that the line ratios are themselves metallicity-dependent; i.e., $I([\text{S II}])/I(\text{H}\alpha)$ decreases with decreasing metallicity.

Hodge 12 has been long known as an SNR (e.g., D’Odorico et al. 1980; D’Odorico & Dopita 1983; Kong et al. 2004). Smith (1975) obtained spectroscopy and found flux ratios $[\text{S II}]/\text{H}\alpha = 0.5$ and $[\text{O III}]/\text{H}\beta = 0.9$. Our two-dimensional spectrum of Hodge 12 and the resulting extracted one-dimensional spectrum are shown in Figs. 7 and 8, respectively. Our measurements (Table 5a) are in general agreement with published line ratios: $I([\text{O III}] \lambda\lambda 4959, 5007)/I(\text{H}\beta) \simeq 0.8$, $I([\text{O I}] \lambda 6363)/I(\text{H}\beta) \simeq 0.2$, $I([\text{N II}] \lambda 6583)/I(\text{H}\alpha) \simeq 0.09$, and $I([\text{S II}])/I(\text{H}\alpha) \simeq 0.5$. Using the grid of SNR models from Dopita et al. (1984, Fig. 8) and our $I([\text{S II}])/I(\text{H}\alpha)$ value, we estimate an oxygen abundance of $12+\log(\text{O}/\text{H}) \simeq 7.9 \pm 0.1$, although our $I([\text{O II}] \lambda 3727)/I(\text{H}\beta)$ and $I([\text{O III}] \lambda\lambda 4959, 5007)/I(\text{H}\beta)$ ratios are, respectively, higher and lower than the ranges expressed in their models. The error in the oxygen abundance is an estimate of the possible range of values obtained from the models.

There are possible SNR among the observed ionized nebulae. The nebulae KD 20 (identified as C10 by Chandar et al. 2000) has an $I([\text{S II}])/I(\text{H}\alpha)$ ratio of 0.4, which is roughly four times larger than the value for a typical H II region in NGC 6822. This excess $[\text{S II}]$ emission is likely the signature of the presence of an SNR. Note that the canonical ratio of 0.5 was established for solar metallicities, and at lower metallicities, $[\text{S II}]$ emission in a photoionized region is smaller; so, $I([\text{S II}])/I(\text{H}\alpha)$ ratios below one-half can still indicate the presence of shock excitation in metal-poor galaxies (Skillman 1985). The nebula KD 12 (identified as C9 by Chandar et al. 2000), although not measured here in the present work, has a similar value of $I([\text{S II}])/I(\text{H}\alpha)$, and is likely another SNR. In the absence of measured $[\text{N II}]$, we adopt the oxygen abundance for KD 12 measured by Chandar et al. (2000) as a lower limit.

3.3. Element Ratios

We briefly discuss argon-to-oxygen, nitrogen-to-oxygen, and neon-to-oxygen ratios, which are listed in Tables 6a and 6b. The following discussion can be referred to Fig. 11.

We derived nitrogen-to-oxygen ratios for three H II regions with $[\text{O III}] \lambda 4363$ and $[\text{N II}] \lambda 6583$ measurements: Hubble V, K α , and KD 28e. Although $[\text{N II}] \lambda 6583$ is blended with $\text{H}\alpha$ in our low-dispersion spectra, we used the IRAF `splot` routine to deblend and measure their line fluxes. For metal-poor galaxies, it is assumed that $\text{N}/\text{O} \approx \text{N}^+/\text{O}^+$ (Garnett 1990) and N^+/O^+ values were derived. Nitrogen abundances were computed as $\text{N}/\text{H} = \text{ICF}(\text{N}) \times (\text{N}^+/\text{H})$. The ionization correction factor, $\text{ICF}(\text{N}) = \text{O}/\text{O}^+$, accounts for missing ions. The resulting nitrogen-to-oxygen abundance ratios were found to be the same as the N^+/O^+ values. From the measurements of the three H II regions, mean values are: $\text{N}/\text{O} = 0.012 \pm 0.001$, and $\log(\text{N}/\text{O}) = -1.92 \pm 0.04$. The latter is significantly lower than the mean for metal-poor blue compact dwarf galaxies ($\log(\text{N}/\text{O}) = -1.46 \pm 0.14$ for galaxies with $12+\log(\text{O}/\text{H}) \gtrsim 7.6$; Izotov & Thuan 1999). Such low values of N/O are not found at all within the sample of blue compact dwarf galaxies by Izotov & Thuan (1999), although some objects with similar N/O ratios are found in the compilation from the literature by Kobulnicky & Skillman (1996). van Zee et al. (1997a; 1997b) have found similarly low values

of N/O in low surface brightness galaxies, although Izotov & Thuan (1999) have questioned the quality of these data.

Skillman et al. (1989) proposed that the low N/O value in NGC 6822 could be attributed to a recent burst of star formation, and can be explained by the time delay between the release of newly synthesized oxygen from massive stars and newly synthesized nitrogen from intermediate mass stars. This was motivated in part by the discovery of a period of star cluster formation about 100 Myr ago (Hodge 1980). Gallart et al. (1996c) used extensive color-magnitude diagram analysis of NGC 6822 to determine the occurrence of an enhanced episode of star formation between 100 and 200 Myr ago. The hypothesis that relatively low N/O observed in NGC 6822 is real and due to its history of star formation history appears to be supported by earlier observations of low N/O values (Pagel et al. 1980; Skillman et al. 1989) and by the low values in three different nebulae from the present study. However, we caution the reader that the present N/O values were derived from low-dispersion spectra with $\text{H}\alpha$ and $[\text{N II}] \lambda 6583$ blended in a number of the spectra (see Figs. 6 and 8). The larger N/O values reported by Peimbert et al. (2005) (in better agreement with the mean value for blue compact dwarf galaxies) were derived from higher-dispersion spectra obtained with the VLT. Due to the importance of the proper interpretation of the N/O values with the recent history of star formation, the N/O values should be confirmed.

Neon abundances are derived as $\text{Ne}/\text{H} = \text{ICF}(\text{Ne}) \times (\text{Ne}^{+2}/\text{H}^{+})$. The ionization correction factor for neon is $\text{ICF}(\text{Ne}) = \text{O}/\text{O}^{+2}$. The mean is $\log(\text{Ne}/\text{O}) = -0.59 \pm 0.12$, which is just in agreement with the mean value of -0.72 ± 0.06 for blue compact dwarf galaxies (Izotov & Thuan 1999)¹⁰. Since the $F([\text{Ne III}] \lambda 3869)/F([\text{O III}] \lambda 5007)$ ratio is sensitive to the reddening correction, and our reddening corrections are only based on the $F(\text{H}\alpha)/F(\text{H}\beta)$ ratio, we revisited this correction method. We have used only reddenings derived using $F(\text{H}\alpha)/F(\text{H}\beta)$ in spectra where $[\text{O III}] \lambda 4363$ was detected. If the $F(\text{H}\alpha)/F(\text{H}\beta)$ is too large, $F([\text{Ne III}] \lambda 3869)/F(\text{H}\beta)$ may be overcorrected. In the spectra for H II regions Hubble V, K α , K β , and KD 28e, high-order unblended Balmer lines (H9, H10, and H11) were detected. The intensity ratios with respect to $\text{H}\beta$ were found to be consistent with expected values for H II regions having electron temperatures in the range between 11500 and 14000 K. In the blue spectrum for H II region Hubble I, we did not detect the higher-order Balmer lines as above. The unblended corrected Balmer line closest to $[\text{Ne III}] \lambda 3869$ is $\text{H}\delta$, because $\text{H}8$ is blended with an adjacent helium line, and $\text{H}\epsilon$ is blended with adjacent $[\text{Ne III}]$ and helium lines. We found that the resulting $I(\text{H}\delta)/I(\text{H}\beta)$ and $I(\text{H}\gamma)/I(\text{H}\beta)$ ratios were consistent with expected Balmer ratios at a temperature $T_e(\text{O}^{+2})$ of about 13000 K.

Argon is more complex, because the dominant ion is not found in just one zone. Ar^{+2} is likely to be found in an intermediate area between the O^+ and O^{+2} zones. Argon abundances were derived using the prescription by Thuan et al. (1995). If only $[\text{Ar III}]$ is present, the argon abundance is $\text{Ar}/\text{H} = \text{ICF}(\text{Ar}) (\text{Ar}^{+2}/\text{H}^{+})$, and the ionization correction fac-

¹⁰ Note that part of the difference is due to a 14% difference in the ratio of the $[\text{O III}] \lambda 5007$ and $[\text{Ne III}] \lambda 3869$ emissivities used by Izotov & Thuan (1999) and that computed by the `IONIC` task in the `NEBULAR` code of Shaw & Dufour (1995). This 14% difference, which translates into a 0.06 dex difference (in the sense observed), is probably an indication of the minimum systematic uncertainty in the atomic data which are used for calculating nebular abundances (see Garnett 2004).

tor is given by $\text{ICF}(\text{Ar}) = \text{Ar}/\text{Ar}^{+2} = [0.15 + x(2.39 - 2.64x)]^{-1}$, where $x = \text{O}^+/\text{O}$. Where $[\text{Ar IV}]$ is also present, the argon abundance is $\text{Ar}/\text{H} = \text{ICF}(\text{Ar}) ((\text{Ar}^{+2} + \text{Ar}^{+3})/\text{H}^+)$, and the ionization correction factor is given by $\text{ICF}(\text{Ar}) = \text{Ar}/(\text{Ar}^{+2} + \text{Ar}^{+3}) = \{0.99 + x[0.091 + x(-1.14 + 0.077x)]\}^{-1}$. Our mean value of $\log(\text{Ar}/\text{O}) = -2.10 \pm 0.06$ is in agreement with the average for metal-poor blue compact dwarf galaxies (Izotov & Thuan 1999).

Moore et al. (2004) has recently suggested that direct modeling of photoionized nebulae should be used to infer elemental abundances with accuracies similar to observations. Abundances derived from model-based ionization correction factors were shown to exceed the range of expected errors from the original data.

4. INTERSTELLAR MEDIUM AND STELLAR OXYGEN ABUNDANCES IN NGC 6822

A compilation of measured oxygen abundances from H II regions, planetary nebulae, and stars from the present work and from the literature is presented in Table 7. To ascertain the possibility of spatial variations in oxygen abundance across the galaxy, we first discuss how radial gradients are derived, followed by a discussion of recent studies in the literature. We examine our highest-quality results in the context of the best data reported in the literature. We will then discuss how the existence of a nonzero radial abundance gradient and a zero gradient can be interpreted from the data, keeping in mind the relative dispersion in oxygen abundances used for the radial fits.

Deprojected galactocentric radii were derived similar to the method described in Venn et al. (2001). We have used the coordinates of the H I dynamical center, position angle, and inclination obtained by Brandenburg & Skillman (1998); these values are also listed in Table 1. Some of the values of the deprojected galactocentric radii reported in Table 7 are different from those reported in Venn et al. (2001) due to a transcription error in the latter work. We note also that the H II region identified as the “nucleus” in Pagel et al. (1980) is likely to be the SNR Hodge 12.

We adopt $r_{\text{exp}} = 3.0 \pm 0.1$ as the exponential scale length from the carbon star survey by Letarte et al. (2002). Carbon stars are a good tracer of the intermediate- to old-age stellar populations, and we assume that the exponential scale length derived by Letarte et al. (2002) is a fair measure of the spatial extent of the underlying stellar population. Thus, we have measured spectra of H II regions out to radii of almost 4.4 scale lengths. Mateo (1998) lists a scale length 2.4 ± 0.4 , based on the observations by Hodge et al. (1991). Using the Hodge et al. value for the exponential scale length would mean that we have covered H II regions out to 5.5 scale lengths.

For a proper comparison with the present data, data for a number of H II regions were reanalyzed. Abundances for Hodge 10, K γ , and Hubble X were rederived using the data from Chandar et al. (2000) and Peimbert et al. (2005); our oxygen abundances agree with the published results. Where there is more than one published measurement for an H II region which we have also measured here, we adopt our derived oxygen abundance, as indicated in Table 7.

4.1. Is There An Abundance Gradient in NGC 6822?

In Fig. 12, we have plotted oxygen abundances for all 19 nebulae in the present work as a function of physical galactocentric radius. The intrinsic errors associated with bright-

line abundances are of order 0.05 dex; in this plot, we have assigned 0.20 dex uncertainties from the bright-line method. In addition to the stellar abundances from Venn et al. (2001), we have also plotted oxygen abundances reported by Smith (1975), Lequeux et al. (1979), Pagel et al. (1980), Skillman et al. (1989), Richer & McCall (1995), Miller (1996), Chandar et al. (2000), Hidalgo-Gómez et al. (2001), Lee et al. (2003d), and Peimbert et al. (2005). Oxygen abundances for H II regions at radii $\lesssim 0.5$ kpc are in agreement with abundances derived for A-type supergiants at similar radii. Most of our derived oxygen abundances for H II regions at “intermediate” radii (≈ 1 kpc; i.e., Hubble V) agree with previously reported values in the literature. Our oxygen abundances for Hubble I and Hubble III also agree with the values determined by Pagel et al. (1980).

There are, however, three data points which suggest significantly lower oxygen abundances. From Chandar et al. (2000), they are K β , KD 12 (C9), and KD 20 (C10); all three are labelled in Fig. 12. For KD 12, Chandar et al. (2000) reported weak $[\text{O III}] \lambda\lambda 4959, 5007$ emission and no $[\text{O III}] \lambda 4363$. Although we have not repeated a measurement for this nebula, simply applying the bright-line method to their published line ratios in the limit of zero reddening yields an oxygen abundance approximately equal to $12 + \log(\text{O}/\text{H}) = 8.3$, which is 0.5 dex higher than their quoted value. The larger oxygen abundance is in better agreement with abundances of other nebulae at comparable radii. Thus, we adopt a lower limit of $12 + \log(\text{O}/\text{H}) \gtrsim 7.8$ for KD 12. In K β , we measured $[\text{O III}] \lambda 4363$, and the derived oxygen abundance is consistent with the (bright-line) abundances derived for H II regions at similar radii (e.g., HK 16, HK 42, KD 9). We have subsequently adopted our $[\text{O III}] \lambda 4363$ oxygen abundance for K β . For KD 20, $[\text{O III}] \lambda 4363$ was neither detected in the present work nor by Chandar et al. (2000); thus, we have adopted a lower limit on the oxygen abundance based on the $[\text{O II}]$ emission.

Oxygen abundances for the two planetary nebulae measured by Richer & McCall (1995) (Fig. 4; Table 7) are slightly lower than the H II region oxygen abundances at similar radii. However, planetary nebulae sample conditions that were present about 1 Gyr ago in the interstellar medium, and the gas should be less metal-rich at that time. Accounting for the effects of mixing on the oxygen abundance during the evolution of the progenitor star are additional complications which are beyond the scope of the present work.

Various linear least-square fits to subsets of abundance data are described and shown in Table 8 and Fig. 13. When all of the 19 measured nebulae (out to four exponential scale lengths) are included in the fit, no clear signature is found for a radial abundance gradient. Including the three stellar abundances also produces zero slope. A slope of -0.14 ± 0.07 dex kpc^{-1} is obtained with a fit to the five H II regions with measured $[\text{O III}] \lambda 4363$; the slope is consistent with zero at 2σ . A fit to just the three A-type supergiants yields a significant slope; such a small sample can clearly bias the resulting fit. If we consider only the five H II regions in the present data with $[\text{O III}] \lambda 4363$ abundances and three additional H II regions with $[\text{O III}] \lambda 4363$ measurements from the literature (Hodge 10 and K γ from Chandar et al. 2000; Hubble X from Peimbert et al. 2005), we obtain

$$12 + \log(\text{O}/\text{H}) = (8.23 \pm 0.05) + (-0.16 \pm 0.05)R, \quad (2)$$

where R is the deprojected galactocentric radius in kpc, and the slope is in units of dex kpc^{-1} . The fit corresponding to Equation (2) is seen in panel (e) of Fig. 13 and is listed as

dataset (e) in Table 8. We remind the reader that despite only eight H II regions, we have culled the best available data at the present time. This slope is slightly more significant (3.2σ), and is about two times larger than that found for the Milky Way (Rolleston et al. 2000), although the value approaches the range observed in other spiral galaxies (e.g., Vila-Costas & Edmunds 1992; Zaritsky et al. 1994). To convert the slope in units of dex kpc⁻¹ to units of dex arcmin⁻¹ and dex r_{exp}^{-1} , we use the linear-to-angular scale for a distance of 0.5 Mpc and the scale length from Table 1, and multiply the derived slopes in Table 8 by 0.144 and 0.432, respectively. The slope above in Equation (2) would thus be -0.023 dex arcmin⁻¹ and -0.069 dex r_{exp}^{-1} . Finally, a fit to the eight H II regions with [O III] $\lambda 4363$ oxygen abundances and three A-type supergiants gives a slope of -0.24 ± 0.07 dex kpc⁻¹ and a zero-point oxygen abundance equal to $12+\log(\text{O}/\text{H}) = 8.34 \pm 0.07$.

4.2. Recent Studies

Vila-Costas & Edmunds (1992) included NGC 6822 in their sample of spiral galaxies to examine the relationship between abundance gradients and other global parameters. They used the data for seven H II regions from Smith (1975) and Pagel et al. (1980), and determined a slope -0.042 dex kpc⁻¹ and a central abundance of $12+\log(\text{O}/\text{H}) = 8.24$. While their result is consistent with zero slope, these data were obtained with photon counters prone to nonlinear behavior (i.e., Jenkins 1987).

Hidalgo-Gómez et al. (2001) suggested the existence of a radial gradient in nebular oxygen abundances, based on small scale variations within the bright H II regions Hubble V and Hubble X. While differences between H II regions were not found, variations as large as ~ 0.4 dex were claimed on physical scales as small as 4 pc within a given H II region. These may be due to either true abundance variations or small-scale temperature changes, but the authors could not distinguish either scenario from their data. Curiously, they report for Hubble V a $\text{H}\alpha/\text{H}\beta$ flux ratio of 1.50 ± 0.07 , which is significantly lower than expected Balmer ratios for typical conditions found in metal-poor H II regions.

Venn et al. (2001) discussed the possibility of an abundance gradient, based on their measurements of oxygen abundances from two A-type supergiants and [O III] $\lambda 4363$ measurements in H II regions, including the data from Pagel et al. (1980) and Skillman et al. (1989). They showed that the abundance gradient was -0.18 dex kpc⁻¹ from a fit to the two A-type supergiants and the [O III] $\lambda 4363$ detections from Pagel et al. (1980). Pilyugin (2001) reevaluated the metallicity-luminosity relation for dwarf irregulars using his empirical method to derive oxygen abundances. He also examined the possibility of an abundance gradient in NGC 6822 by deriving empirical oxygen abundances using data from Lequeux et al. (1979), Pagel et al. (1980), Skillman et al. (1989), and Hidalgo-Gómez et al. (2001). Fitting the empirical abundances and the two stellar abundances from Venn et al. (2001), the resulting slope was -0.035 dex kpc⁻¹, claimed to be consistent with zero slope.

Peimbert et al. (2005) obtained high quality VLT spectra of the H II regions Hubble V and Hubble X. They examined the data for possible temperature fluctuations (Peimbert 1967), which could give rise to small-scale chemical inhomogeneities. They observed recombination and collisionally-excited lines in the giant H II region Hubble V. They derived a recombination-line oxygen abundance $12+\log(\text{O}/\text{H}) = 8.37 \pm 0.09$, which is in better agreement with the mean oxy-

gen abundance for the two A-type supergiants ($12+\log(\text{O}/\text{H}) = 8.36 \pm 0.19$; Venn et al. 2001). From the collisionally-excited emission lines, they derived $12+\log(\text{O}/\text{H}) = 8.08 \pm 0.03$ and 8.34 ± 0.06 for zero and non-zero temperature fluctuations, respectively. Our direct oxygen abundance (8.14 ± 0.05) agrees with their collisional-line abundance derived with zero temperature fluctuations. For Hubble X, they were unable to observe the oxygen recombination lines, and derived oxygen abundances from collisionally-excited lines of 8.01 ± 0.05 and 8.19 ± 0.16 for zero and non-zero temperature fluctuations, respectively. We rederived oxygen abundances using their reported fluxes with our two-zone model and with zero temperature fluctuations. We obtained $12+\log(\text{O}/\text{H}) = 8.11$ and 8.06 for Hubble V and Hubble X, respectively, which agree with their published values. However, for Hubble V we derived $T_e(\text{O}^+) = 11200 \pm 750$ K, while they reported 13000 ± 1000 K. This is a significant difference, especially considering that the values of $T_e(\text{O}^{+2})$ are in excellent agreement. It is interesting to note that their N/O values ($\log(\text{N}/\text{O}) \approx -1.3$) are more in line with the values expected for their oxygen abundances in comparison to other metal-poor galaxies. To compare the present nebular data with other published work, we have only considered their collisional-line abundances, and assumed zero temperature fluctuations. We note that Carigi et al. (2005) have recently described a suite of chemical evolution models, which agree with the photometric properties and the star-formation history of NGC 6822.

4.3. Abundance Variations: The Dispersion in Oxygen Abundance

If we assume zero radial gradient, we derive a mean nebular oxygen abundance for the H II regions with [O III] $\lambda 4363$ measurements. We obtained [O III] $\lambda 4363$ detections in both grating settings for H II regions Hubble V, K α , and KD28e; we computed a single average for each of these three H II regions. The mean oxygen abundance for Hubble V, K α , K β , Hubble I, and K γ is $(\text{O}/\text{H}) = (1.29 \pm 0.30) \times 10^{-4}$, or $12+\log(\text{O}/\text{H}) = 8.11 \pm 0.10$ ($^{+0.08}_{-0.14}$). For the logarithmic value, the two errors represent the overall dispersion in the mean, and the distribution of minimum and maximum values, respectively. The mean value corresponds to $[\text{O}/\text{H}] = -0.55$ dex, or 28% of the solar value. For historical completeness, our adopted mean nebular oxygen abundance would correspond to $[\text{O}/\text{H}] = -0.83$ for a solar value of $12+\log(\text{O}/\text{H}) = 8.93$ stated by Anders & Grevesse (1989). If we include the three additional H II regions with recent [O III] $\lambda 4363$ measurements (Hodge 10 and K γ from Chandar et al. 2000; Hubble X from Peimbert et al. 2005), the mean oxygen abundance is $12+\log(\text{O}/\text{H}) = 8.08 \pm 0.09$ ($^{+0.11}_{-0.10}$). The mean oxygen abundance is consistent with abundances for nearby dwarf irregular galaxies at comparable optical luminosities (e.g., Skillman et al. 1989; Richer & McCall 1995; Lee et al. 2003b). A reexamination of the various fits in Fig. 13 shows that the largest dispersion ($\lesssim 0.2$ dex) occurs when the bright-line abundances are included in the fit which results in zero slope. This is no surprise, as the relative differences between direct and bright-line abundances is about 0.2 dex (see Fig. 10). This argues for relative chemical homogeneity to the level of about 0.2 dex over scales spanning over four exponential scale lengths ($\gtrsim 2$ kpc).

However, we have seen that a subset with the highest quality ([O III] $\lambda 4363$ measurements) suggests an abundance gradient. Is the gradient related to the extended spatial distributions of H I gas and blue stars? The blue stars are too old (\approx

100–200 Myr; de Blok & Walter 2003; Komiyama et al. 2003) to affect the most recent chemical enrichment found in H II regions. Is the gradient caused by H I dilution at large galactocentric radius? The H I cloud to the northwest of NGC 6822 and the overall unusual spatial distribution of H I (de Blok & Walter 2000, 2005) may be diluting the present-day chemical enrichment in the outlying regions of the galaxy, which could give rise to the gradient observed.

Additional measurements would clearly be valuable, although there are no H II regions as bright as Hubble V at large galactocentric radii. While the H II region KD 28 ($R/r_{\text{exp}} \approx 4.4$) anchors the slope at large galactocentric radii, only bright nebular emission lines were observed for this faint diffuse H II region. What is very interesting is that KD 28 is located where a spur of young blue stars extends from the southeast corner of the optical bar (e.g., de Blok & Walter 2003; Komiyama et al. 2003). A closer inspection of the Local Group Survey H α image reveals a number of *compact* emission-line regions in the vicinity of KD 28. de Blok & Walter (2005) have found additional H II regions at intermediate radii from very deep H α imaging with the INT 2.5-m telescope. Very deep spectra would be required to detect [O III] $\lambda 4363$ for KD 28 (or any of the other H II regions). These data could help secure additional evidence of an abundance gradient at large galactocentric radii.

Spectroscopy of other stellar probes would also provide valuable information. Data for two additional A-type supergiants at intermediate galactocentric radii, which would better bridge the measurements of the other stars at small radii, will be presented in a subsequent paper (Venn et al., in preparation). Additional candidates of A-type supergiants for subsequent spectroscopy would clearly be valuable as an additional probe of the most recent episode of chemical enrichment. Spectroscopy of the confirmed PNe candidates (e.g., Leisy et al. 2005) would also indicate the consistency of abundances at a given radius, and would show whether the interstellar medium about 1 Gyr ago also exhibited overall spatial chemical homogeneity (modulo possible mixing in the progenitor stars). If they are sufficiently luminous, spectroscopy of individual blue stars at large galactocentric radii could provide another valuable test, as the blue stars have ages intermediate to the young H II regions and the (relatively) older PNe. Tolstoy et al. (2001) obtained direct spectroscopic metallicities for 23 red giant stars in NGC 6822 and determined the metallicity distribution function with mean $[\text{Fe}/\text{H}] = -1 \pm 0.5$. This mean iron abundance is similar to the photometric iron abundances of stars (Lee et al. 1993; Gallart et al. 1996b,c) and to the spectroscopic abundances of open clusters (Cohen & Blakeslee 1998) in the galaxy. We have plotted spectroscopic iron abundances of the 23 red giant stars as a function of their galactocentric radius in Fig. 14. There is no signature of a radial gradient in iron abundance for the older stellar population. This is not entirely surprising, as the red giant stars have a larger range of (old) ages than the H II regions. The larger range in age “hides” previous episodes of star formation and the subsequent episodes of chemical enrichment. Continuing work with the VLT for an additional 90 red giant stars in NGC 6822 (A. A. Cole et al., in preparation) could provide stronger constraints on the history of star formation over a larger range of ages.

5. CONCLUSIONS

Optical spectra were measured for 19 nebulae in NGC 6822 at galactocentric radii between 0.05 kpc and 2 kpc, or out to about four exponential scale lengths. [O III] $\lambda 4363$ was detected in five H II regions, and subsequent direct oxygen abundances were derived. Oxygen abundances for the remaining H II regions were derived using bright-line methods. Oxygen abundances for the A-type supergiant stars are consistent with H II region abundances at comparable galactocentric radii. Linear least-square fits to various subsets of abundance data were obtained. When all of the measured nebulae are included, no clear signature is found for an abundance gradient out to over four exponential scale lengths. A fit to H II regions with only [O III] $\lambda 4363$ detections is consistent with zero slope (2σ). The abundance gradient becomes slightly more significant (3.2σ) when three additional H II regions with [O III] $\lambda 4363$ measurements from the literature are included. The resulting slope and extrapolated central abundance are -0.16 ± 0.05 dex kpc^{-1} and $12 + \log(\text{O}/\text{H}) = 8.23 \pm 0.05$, respectively. Assuming zero abundance gradient, we take the five H II regions with [O III] $\lambda 4363$ detections from our present work, and derive a mean nebular oxygen abundance $12 + \log(\text{O}/\text{H}) = 8.11 \pm 0.10$, which corresponds to $[\text{O}/\text{H}] = -0.55$. Additional deep high-quality spectra of nebulae and stars are required to distinguish clearly between either a zero or a non-zero slope. The latter would be confirmation of an abundance gradient seen for the first time in a dwarf irregular galaxy.

We thank the anonymous referee for their careful reading and their helpful comments which improved the presentation of the manuscript. H. L. thanks Fabio Bresolin, John Cannon, Maria-Rosa Cioni, Andrew Cole, Erwin de Blok, Ana Maria Hidalgo-Gómez, Pierre Leisy, Laura Magrini, Lissa Miller, Erik Muller, Michael Richer, Jeroen Stil, and Marc Zimer for helpful and informative exchanges. We thank Antonio Peimbert, Manuel Peimbert, and Leticia Carigi for copies of their manuscripts before publication. We are grateful to ESO for awarded telescope time, and H. L. thanks Lisa Germany and the staff at ESO La Silla for their help in acquiring the data. H. L. and E. D. S. acknowledge partial support from a NASA LTSARP grant NAG 5–9221 and the University of Minnesota. K. A. V. thanks the National Science Foundation for support through a CAREER award AST 99–84073. For their one-year visit, E. D. S. and K. A. V. thank the Institute of Astronomy, University of Cambridge for their hospitality and support. Some data were accessed as Guest User, Canadian Astronomy Data Center, which is operated by the Dominion Astrophysical Observatory for the National Research Council of Canada’s Herzberg Institute of Astrophysics. This research has made use of NASA’s Astrophysics Data System, and of the NASA/IPAC Extragalactic Database, which is operated by the Jet Propulsion Laboratory, California Institute of Technology, under contract with the National Aeronautics and Space Administration.

Facility: ESO:3.6m (EFOSC2)

REFERENCES

- Allain, D. 1974, *A&A*, 33, 337
 Anders, E., & Grevesse, N. 1989, *Geochim. Cosmochim. Acta*, 53, 197
 Asplund, M., Grevesse, N., Sauval, A. J., Allende Prieto, C., & Kiselman, D. 2004, *A&A*, 417, 751

- Baldwin, J. A., Phillips, M. M., & Terlevich, R. 1981, *PASP*, 93, 5
- Battinelli, P., Demers, S., & Letarte, B. 2003, *A&A*, 405, 563
- Brandenburg, H. J., & Skillman, E. D. 1998, *BAAS*, 30, 1354
- Campbell, A., Terlevich, R., & Melnick, J. 1986, *MNRAS*, 223, 811
- Carigi, L., Colin, P., & Peimbert, M. 2005, *ApJ*, submitted (astro-ph/0509829)
- Chandar, R., Bianchi, L., & Ford, H. C. 2000, *AJ*, 120, 3088
- Cioni, M.-R. L., & Habing, H. J. 2005, *A&A*, 429, 837
- Clementini, G., Held, E. V., Baldacci, L., & Rizzi, L. 2003, *ApJ*, 588, L85
- Cohen, J. G., & Blakeslee, J. P. 1998, *AJ*, 115, 2356
- de Blok, W. J. G., & Walter, F. 2000, *ApJ*, 537, L95
- de Blok, W. J. G., & Walter, F. 2003, *MNRAS*, 341, L39
- de Blok, W. J. G., & Walter, F. 2005, *AJ*, in press (astro-ph/0508018)
- Dinerstein, H. L. 1990, in *The Interstellar Medium in Galaxies*, ed. H. A. Thronson & J. M. Shull (Dordrecht: Kluwer), 257
- D’Odorico, S., Dopita, M. A., & Benvenuti, P. 1980, *A&AS*, 40, 67
- D’Odorico, S., & Dopita, M. A. 1983, in *IAU Symp. 101: Supernova Remnants and their X-ray Emission*, eds. J. Danziger & P. Gorenstein (Dordrecht, Boston), 517
- Dopita, M. A., Binette, L., D’Odorico, S., & Benvenuti, P. 1984, *ApJ*, 276, 653
- Dufour, R. J., & Talent, D. L. 1980, *ApJ*, 235, 22
- Gallart, C., Aparicio, A., Bertelli, G., & Chiosi, C. 1996a, *AJ*, 112, 1928
- Gallart, C., Aparicio, A., Bertelli, G., & Chiosi, C. 1996b, *AJ*, 112, 1950
- Gallart, C., Aparicio, A., Bertelli, G., & Chiosi, C. 1996c, *AJ*, 112, 2596
- Garnett, D. R. 1990, *ApJ*, 363, 142
- Garnett, D. R. 1992, *AJ*, 103, 1330
- Garnett, D. R. 2004, in *Cosmochemistry: The Melting Pot of the Elements*, XIII Canary Islands Winter School of Astrophysics, eds. C. Esteban, R. J. García-López, A. Herrero, & F. Sánchez (Cambridge: Cambridge University Press), 171
- Hidalgo-Gómez, A. M., Olofsson, K., & Masegosa, J. 2001, *A&A*, 367, 388
- Hodge, P. W. 1980, *ApJ*, 241, 125
- Hodge, P. W., Kennicutt, R. C., Jr., & Lee, M. G. 1988, *PASP*, 100, 917
- Hodge, P. W., Smith, T., Eskridge, P., MacGillivray, H., & Beard, S. 1991, *ApJ*, 379, 621
- Huchtmeier, W. K., & Richter, O. G. 1986, *A&AS*, 63, 323
- Hutchings, J. B., Cavanagh, B., & Bianchi, L. 1999, *PASP*, 111, 559
- Izotov, Y. I., & Thuan, T. X. 1999, *ApJ*, 511, 639
- Jenkins, C. R. 1987, *MNRAS*, 226, 341
- Karachentsev, I. D., Karachentseva, V. E., Huchtmeier, W. K., & Makarov, D. I. 2004, *AJ*, 127, 2031
- Kaufer, A., Venn, K. A., Tolstoy, E., Pinte, C., & Kudritzki, R. P. 2004, *AJ*, 127, 2723
- Killen, R. M., & Dufour, R. 1982, *PASP*, 94, 444
- Kobulnicky, H. A., & Skillman, E. D. 1996, *ApJ*, 471, 211
- Kobulnicky, H. A., & Skillman, E. D. 1997, *ApJ*, 489, 636
- Kobulnicky, H. A., Kennicutt, R. C. Jr., & Pizagno, J. L. 1999, *ApJ*, 514, 544
- Komiyama, Y. et al. 2003, *ApJ*, 590, L17
- Kong, A. K. H., Sjouwerman, L. O., & Williams, B. F. 2004, *AJ*, 128, 2783
- Krienke, K., & Hodge, P. 2004, *PASP*, 116, 497
- Lee, H. 2001, Ph.D. thesis, York University
- Lee, H., Grebel, E. K., & Hodge, P. W. 2003a, *A&A*, 401, 141
- Lee, H., McCall, M. L., Kingsburgh, R., Ross, R., & Stevenson, C. C. 2003b, *AJ*, 125, 146
- Lee, H., McCall, M. L., & Richer, M. G. 2003c, *AJ*, 125, 2975
- Lee, H., Skillman, E. D., & Venn, K. A. 2003d, *BAAS*, 35, 1393
- Lee, H., & Skillman, E. D. 2004, *ApJ*, 614, 698
- Lee, H., Skillman, E. D., & Venn, K. A. 2005, *ApJ*, 620, 223
- Lee, M. G., Freedman, W. L., & Madore, B. F. 1993, *ApJ*, 417, 553
- Leisy, P., Corradi, R. L. M., Magrini, L., Greimel, R., Mampaso, A., & Dennefeld, M. 2005, *A&A*, 436, 437
- Lequeux, J., Peimbert, M., Rayo, J. F., Serrano, A., & Torres-Peimbert, S. 1979, *A&A*, 80, 155
- Letarte, B., Demers, S., Battinelli, P., & Kunkel, W. E. 2002, *AJ*, 123, 832
- Levenson, N. A., Krishner, R. P., Blair, W. P., & Winkler, P. F. 1995, *AJ*, 110, 739
- Massey, P., Hodge, P. W., Holmes, S., Jacoby, G., King, N. L., Olsen, K., Smith, C., & Saha, A. 2002, *BAAS*, 34, 1272
- Mateo, M. 1998, *ARA&A*, 36, 435
- McCall, M. L., Rybski, P. M., & Shields, G. A. 1985, *ApJS*, 57, 1
- McGaugh, S. S. 1991, *ApJ*, 380, 140
- McGaugh, S. S. 1994, *ApJ*, 426, 135
- Meléndez, J. 2004, *ApJ*, 615, 1042
- Miller, B. W. 1995, *ApJ*, 446, L75
- Miller, B. W. 1996, *AJ*, 112, 991
- Moore, B. D., Hester, J. J., & Dufour, R. J. 2004, *AJ*, 127, 3484
- Muschielok et al. 1999, *A&A*, 352, L40
- Nollenberg, J. G., Skillman, E. D., Garnett, D. R., & Dinerstein, H. L. 2002, *ApJ*, 581, 1002
- Osterbrock, D. E. 1989, *Astrophysics of Gaseous Nebulae and Active Galactic Nuclei* (Mill Valley: University Science Books)
- Pagel, B. E. J., Edmunds, M. G., Blackwell, D. E., Chen, M. S., & Smith, G. 1979, *MNRAS*, 189, 95
- Pagel, B. E. J., Edmunds, M. G., & Smith, G. 1980, *MNRAS*, 193, 219
- Peimbert, A., Peimbert, M., & Ruiz, M. T. 2005, *ApJ*, 634, 1056
- Peimbert, M. 1967, *ApJ*, 150, 825
- Peimbert, M., & Spinrad, H. 1970, *A&A*, 7, 311
- Pietrzyński, G., Gieren, W., Udalski, A., Bresolin, F., Kudritzki, R., Soszyński, I., Szymański, M., & Kubiak, M. 2004, *AJ*, 128, 2815
- Pilyugin, L. S. 2000, *A&A*, 362, 325
- Pilyugin, L. S. 2001, *A&A*, 374, 412
- Richer, M. G., & McCall, M. L. 1995, *ApJ*, 445, 642
- Roberts, M. S. 1972, in *IAU Symp. 44, External Galaxies and Quasi-Stellar Objects*, ed. D. S. Evans (Dordrecht: Reidel), 12
- Rollston, W. R. J., Smartt, S. J., Dufton, P. L., & Ryans, R. S. I. 2000, *A&A*, 363, 537
- Russell, S. C., & Dopita, M. A. 1990, *ApJS*, 74, 93
- Shaw, R. A., & Dufour, R. J. 1995, *PASP*, 107, 896
- Skillman, E. D. 1985, *ApJ*, 290, 449
- Skillman, E. D. 1989, *ApJ*, 347, 883
- Skillman, E. D. 1998, in *Stellar Astrophysics of the Local Group: VIII Canary Islands Winter School of Astrophysics*, ed. A. Aparicio, A. Herrero, & F. Sánchez (Cambridge: Cambridge University Press), 457
- Skillman, E. D., Kennicutt, R. C., Jr., & Hodge, P. 1989, *ApJ*, 347, 875
- Skillman, E. D., Côté, S., & Miller, B. W. 2003, *AJ*, 125, 610
- Skillman, E. D., Terlevich, R., & Melnick, J. 1989, *MNRAS*, 240, 563
- Smith, H. E. 1975, *ApJ*, 199, 591
- Smith, R. C., Kirshner, R. P., Blair, W. P., Long, K. S., & Winkler, P. F. 1993, *ApJ*, 407, 564
- Stasińska, G. 1990, *A&AS*, 83, 501
- Talent, D. L. 1980, Ph.D. thesis, Rice University
- Tenorio-Tagle, G. 1996, *AJ*, 111, 1641
- Thuan, T. X., Izotov, Y. I., & Lipovetsky, V. A. 1995, *ApJ*, 445, 108
- Tolstoy, E., Irwin, M. J., Cole, A. A., Pasquini, L., Gilmozzi, R., & Gallagher, J. S. 2001, *MNRAS*, 327, 918
- van den Bergh, S. 2000, *The Galaxies of the Local Group* (Cambridge: Cambridge University Press)
- van Zee, L., & Haynes, M. P. 2005, submitted
- van Zee, L., Haynes, M. P., & Salzer, J. J. 1997a, *AJ*, 114, 2479
- van Zee, L., Haynes, M. P., & Salzer, J. J. 1997b, *AJ*, 114, 2497
- van Zee, L., Skillman, E. D., & Salzer, J. J. 1998, *AJ*, 116, 1186
- Veilleux, S., & Osterbrock, D. E. 1987, *ApJ*, 63, 295
- Venn, K. A., & Miller, L. 2002, in “Ionized Gaseous Nebulae”, ed. W. Henney, J. Franco, M. Martos, & M. Peña, *Rev. Mex. AA Conference Series* 12, 230
- Venn, K. A., Lennon, D. J., Kaufer, A., McCarthy, J. K., Przybilla, N., Kudritzki, R. P., Lemke, M., Skillman, E. D., & Smartt, S. J. 2001, *ApJ*, 547, 765
- Venn, K. A., Tolstoy, E., Kaufer, A., Skillman, E. D., Clarkson, S. M., Smartt, S. J., Lennon, D. J., & Kudritzki, R. P. 2003, *AJ*, 126, 1326
- Vila-Costas, M. B., & Edmunds, M. G. 1992, *MNRAS*, 259, 121
- Wilson, C. D. 1992, *AJ*, 104, 1374 (erratum: 1995, *AJ*, 109, 449)
- Wyder, T. K. 2001, *AJ*, 122, 2490
- Zaritsky, D., Kennicutt, R. C., & Huchra, J. P. 1994, *ApJ*, 420, 87

FIG. 1.— NGC 6822 : the field of view is about $21'.9 \times 19'.2$. North is at the top and East is to the left. White objects on the image indicate bright sources in the unsubtracted $H\alpha$ image from the Local Group Survey (Massey et al. 2002). Numeric labels indicate subsequent fields of view around Hubble I and III, Hubble V, and the center in Figs. 2 to 4, respectively. Three A-type supergiant stars and two planetary nebulae in the galaxy are indicated with blue and yellow symbols, respectively. The H I dynamical center of NGC 6822 is marked with a cross (Brandenburg & Skillman 1998), and the $10'$ by $7'$ (1.4 kpc by 1.0 kpc) ellipse at a position angle of 112° indicates approximately the orientation of the H I distribution, which extends much farther east-west than what can be shown here (e.g., de Blok & Walter 2000).

FIG. 2.— Long-slit position for blue spectra of H II regions Hubble III (Hu III) and Hubble I (Hu I). The field of view is $2'.7 \times 2'.4$. Orientation is the same as in Figure 1. Resolved features within Hu III and Hu I are labeled for which spectra were obtained. The separation between the solid lines corresponds approximately to the $1''.5$ slit width projected on the sky. The location of an A-type supergiant star, CW 22, in NGC 6822 is indicated.

FIG. 3.— Long-slit positions for spectra in the area around the giant H II region Hubble V (Hu V). The field of view is $2'.7 \times 2'.4$ and the orientation is the same as in Figure 1. The long-slit orientations on 26 Aug (grating 11) and on 31 Aug (grating 7) are labeled. For a given slit position, the separation between the solid lines corresponds approximately to the $1''.5$ slit width projected on the sky. Labeled are H II regions for which spectra were obtained and presented in this work, except Hodge 6 and KD 12 (C9 in Chandar et al. 2000). The locations of the latter two H II regions are provided for clarity.

FIG. 4.— The central $5'.4 \times 4'.8$ field of view of NGC 6822. Orientation is the same as in Figure 1. H II regions, stars, and planetary nebulae are labelled; see Table 7. KD 20 or C10 as labeled by Chandar et al. (2000) is indicated. Two A-type supergiant stars, CW173 and CW175, (Venn et al. 2001), and two planetary nebulae, S16 and S33 (Richer & McCall 1995) are marked. The H I dynamical center (Brandenburg & Skillman 1998) is marked with a cross.

FIG. 5.— Blue spectra of NGC 6822 nebulae: [O III] $\lambda 4363$ detections. The observed flux per unit wavelength is plotted versus wavelength. Within each panel, the full spectrum and an expanded view of the spectrum to highlight faint emission lines are shown. The [O III] $\lambda 4363$ line is indicated by an arrow in each panel.

FIG. 6.— Low-dispersion spectra of NGC 6822 nebulae: [O III] $\lambda 4363$ detections are shown in the first three panels. Comments are the same as in Fig. 5. Note that H II regions KD 28e and KD 28 are not located in the same part of the galaxy. KD 28 is located in the southern periphery of the galaxy (Fig. 1), whereas KD 28e is located near the center of the galaxy (Fig. 4). The spectrum for KD 28 is shown, because this H II region is farthest from the center with a measurement, and anchors the fit at large radii (see Figs. 12 and 13).

FIG. 7.— Two-dimensional spectrum image from [O II] $\lambda 3727$ to [O II] $\lambda\lambda 7320, 7330$: spectra for KD 24, HK 69, and Hodge 12 (Ho 12) are shown. Dark objects on the image indicate bright sources. Key emission lines are labelled; vertical stripes are night-sky lines. The long-slit was positioned so that north was at the top of the frame. Resolved structure is evident in the emission lines for Ho 12.

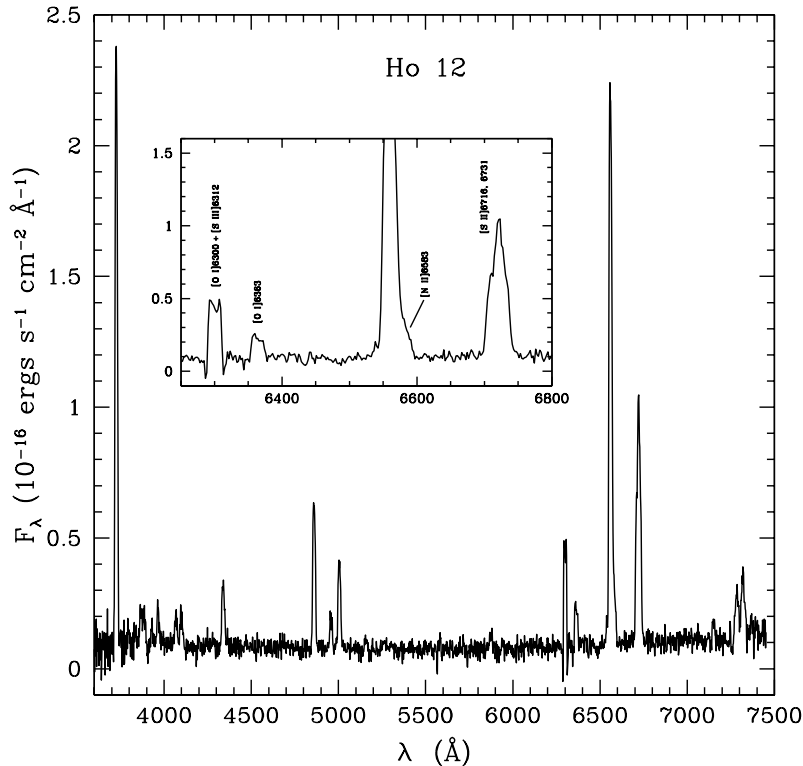


FIG. 8.— Low-dispersion spectrum of the center of Hodge 12. The inset shows the spectrum in the wavelength range between 6250 and 6800 \AA , highlighting relatively bright [O I] $\lambda 6363$ and [S II] $\lambda\lambda 6716, 6731$ emission lines.

FIG. 9.— Monte Carlo simulations of solutions for the reddening, $c(H\beta)$, and the underlying Balmer absorption with equivalent width, EW_{abs} , from hydrogen Balmer flux ratios. Dotted lines mark zero values for each quantity. The results here are shown for the low-dispersion spectrum of Hubble V. Each small point is a solution derived from a different realization of the same input spectrum. The large filled circle with error bars shows the mean result with 1σ errors derived from the dispersion in the solutions. In this example, the Monte Carlo simulations have yielded an unphysical result for the underlying Balmer absorption; thus, we adopt an underlying Balmer absorption with equivalent width equal to zero.

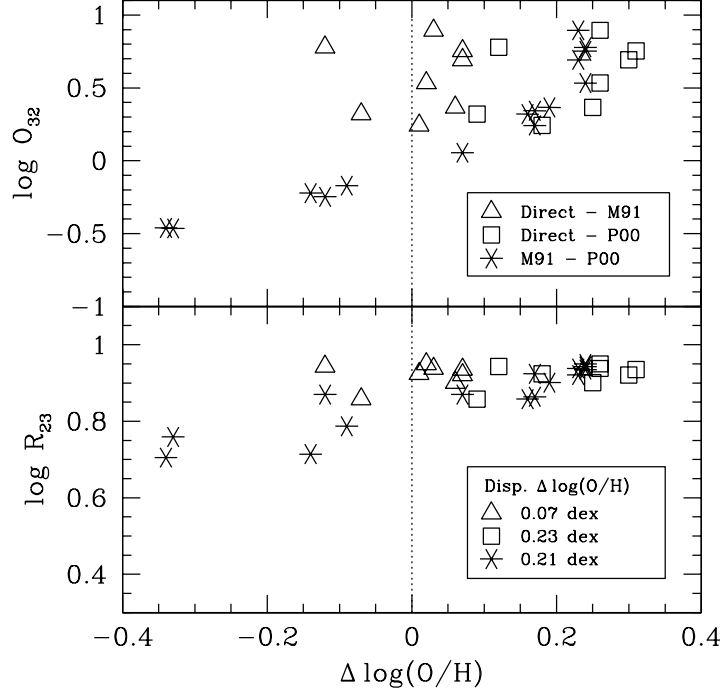


FIG. 10.— Difference in oxygen abundance from various methods versus $\log O_{32}$ (top panel), and versus $\log R_{23}$ (bottom panel). Each symbol represents an H II region. “Direct” denotes oxygen abundances derived from [O III] $\lambda 4363$ measurements, “M91” denotes oxygen abundances derived using the bright-line method by McGaugh (1991), and “P00” denotes oxygen abundances derived using the bright-line method by Pilyugin (2000). Vertical dotted lines in both panels mark zero differences in oxygen abundance. Dispersions in abundance differences are indicated in the legend of the bottom panel. In the absence of [O III] $\lambda 4363$, oxygen abundances derived with the bright-line method are accurate to within ≈ 0.2 dex.

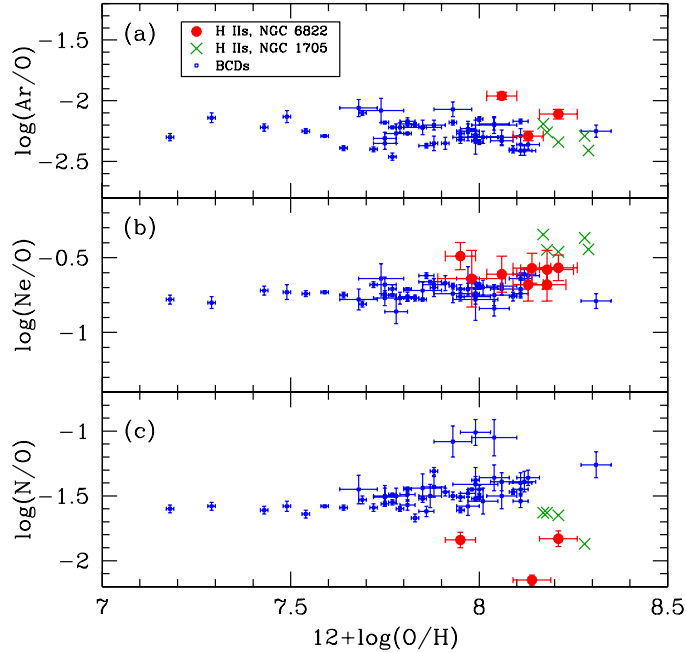


FIG. 11.— Nebular abundance ratios versus oxygen abundance: (a) argon-to-oxygen, (b) neon-to-oxygen, and (c) nitrogen-to-oxygen. Filled circles indicate H II regions in NGC 6822 with [O III] $\lambda 4363$ measurements. Small squares represent blue compact dwarf galaxies (Izotov & Thuan 1999). Crosses indicate H II regions in the starbursting dwarf galaxy NGC 1705 (Lee & Skillman 2004).

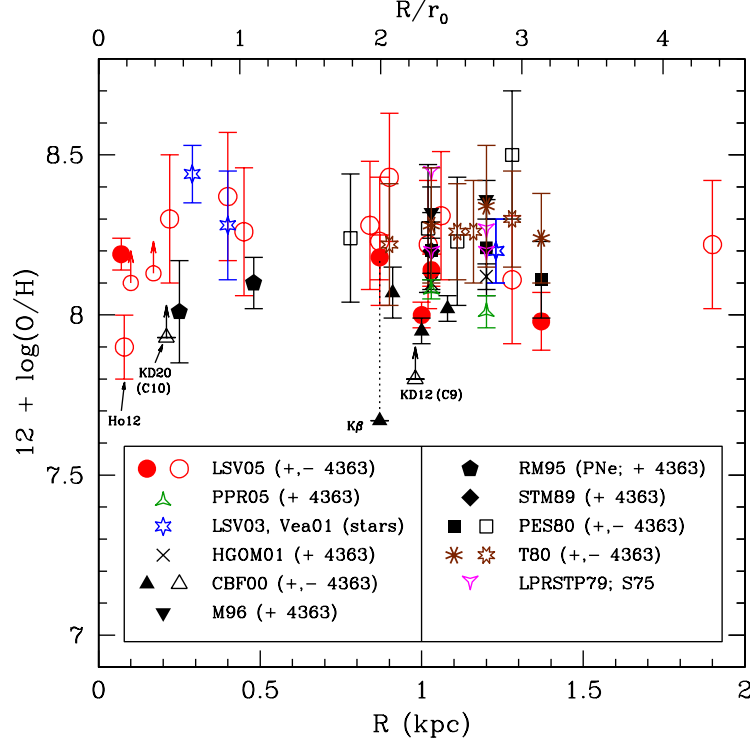


FIG. 12.— Oxygen abundance versus deprojected galactocentric radius. The bottom horizontal axis shows the physical radius in kpc, whereas the top horizontal axis shows the radius normalized by the exponential scale length, r_0 , reported by Letarte et al. (2002). Symbols represent data from the following sources: LSV05 – nebulae from this work; PPR05 – H II regions from Peimbert et al. (2005); LSV03, Vea01 – A-type supergiants from Venn et al. (2001), Venn & Miller (2002), and Lee et al. (2003d); HGOM01 – H II regions from Hidalgo-Gómez et al. (2001); CBF00 – H II regions from Chandar et al. (2000); M96 – H II regions from Miller (1996); RM95 – planetary nebulae from Richer & McCall (1995); STM89 – H II region from Skillman et al. (1989); PES80 – H II regions from Pagel et al. (1980); T80 – H II regions from Talent (1980); LPRSTP79 – H II regions from Lequeux et al. (1979); and S75 – H II regions from Smith (1975). The legend indicates the various symbols representing positive $[\text{O III}] \lambda 4363$ detections in H II regions. The three anomalously low oxygen abundances reported by Chandar et al. (2000) for K β , KD12 (C9), and KD20 (C10) are discussed in the text. A dotted vertical line connects two measurements of the H II region K β ; see text. Also labeled is the supernova remnant Hodge 12 (Ho12).

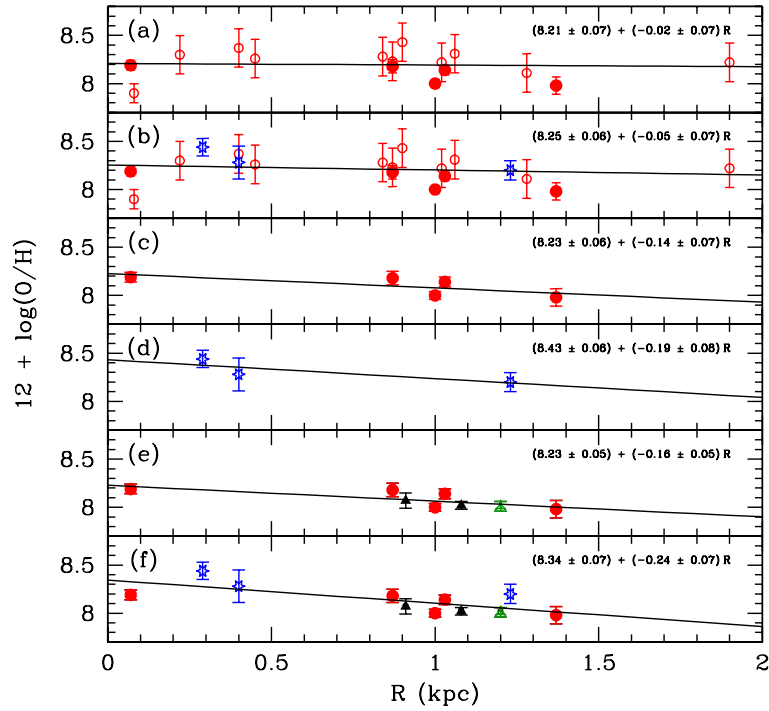


FIG. 13.— Fits to subsets of oxygen abundance data. Symbols and the plot axes for each panel are the same as in Fig. 12. Each panel corresponds to the specific subset of abundance data, and the linear least-squares fit described in Table 8. For nebular [O III] $\lambda 4363$ abundances, we only considered data obtained with CCDs for an appropriate comparison. We adopt oxygen abundances derived for all H II regions which were remeasured in the present work (e.g., our O/H for Hubble V).

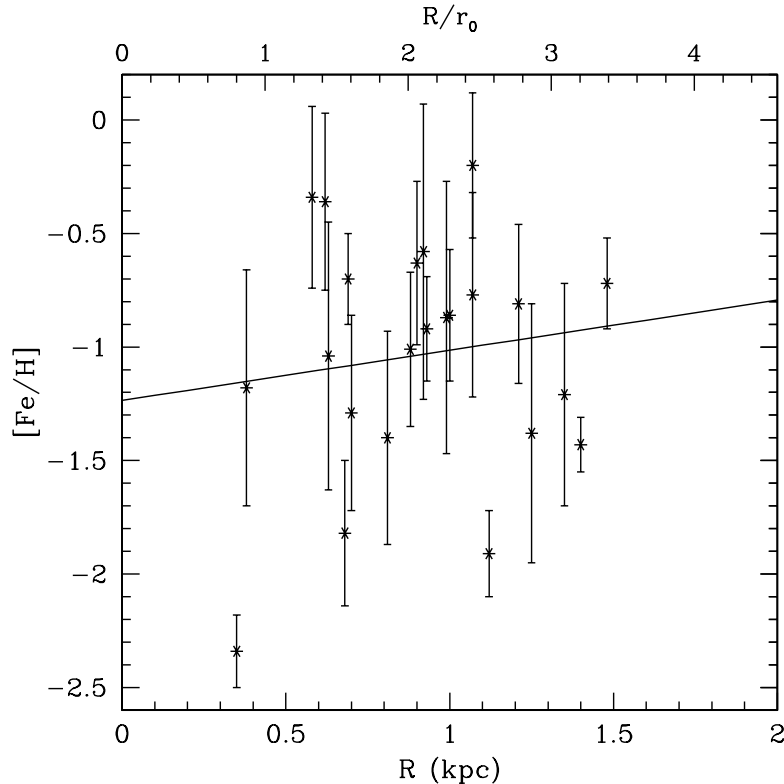


FIG. 14.— Iron abundance, $[\text{Fe}/\text{H}]$, versus deprojected galactocentric radius, R , for 23 red giant stars in the northern half of NGC 6822 (Tolstoy et al. 2001). The resulting least-squares fit is expressed as $[\text{Fe}/\text{H}] = (-1.23 \pm 0.34) + (0.22 \pm 0.35)R$.

TABLE 1
BASIC DATA FOR NGC 6822.

Property	Value	References
Morphological Type	IB(s)m	...
Alternate Names	DDO 209, IC 4895	...
Right ascension (J2000) ^a	19 ^h 44 ^m 56 ^s .4	1
Declination (J2000) ^a	−14° 48′ 04″.5	1
Position angle	112°	1
Inclination	50° 1	1
Distance	0.47–0.50 Mpc	2, 3, 4
Linear to angular scale at this distance	2.3–2.4 pc arcsec ^{−1}	5
Heliocentric velocity	−54 km s ^{−1}	6
r_{exp} , exponential scale length	3′.0 ± 0′.1	7
D_{25} ^b	15′.5	8
B_T ^c	9.32	8
$E(B-V)$ ^c	0.236	8
$M_{B,0}$ ^c	−15.1	5
F_{21} , 21-cm flux integral	2399 Jy km s ^{−1}	8, 9
$\langle 12+\log(\text{O}/\text{H}) \rangle$, A-sg ^d	8.36 ± 0.19 (± 0.21)	10
$\langle 12+\log(\text{O}/\text{H}) \rangle$, H II ^e	8.11 ± 0.10	5
$\Delta[\log(\text{O}/\text{H})]/\Delta R$ ^f	−0.16 ± 0.05 dex kpc ^{−1}	5
$12+\log(\text{O}/\text{H})_c$ ^f	8.23 ± 0.05	5

REFERENCES. — (1) Brandenburg & Skillman (1998); (2) Gallart et al. (1996a); (3) Clementini et al. (2003); (4) Pietrzyński et al. (2004); (5) present work; (6) Mateo (1998); (7) Letarte et al. (2002); (8) Karachentsev et al. (2004); (9) Huchtmeier & Richter (1986); (10) Venn et al. (2001).

^a Coordinates of the H I dynamical center.

^b Major angular diameter measured at 25 mag arcsec^{−2}.

^c Apparent total B magnitude, foreground reddening to the galaxy, and reddening-corrected absolute total B magnitude (0.5 Mpc distance), respectively.

^d Mean stellar oxygen abundance from two A-type supergiant stars.

^e Zero gradient: mean nebular oxygen abundance derived from [O III] $\lambda 4363$ measurements in five H II regions.

^f Non-zero gradient (3.2 σ): slope and extrapolated central oxygen abundance, respectively; see dataset e from Table 8.

TABLE 2
PROPERTIES OF EFOSC2 SPECTROGRAPH EMPLOYED AT THE ESO LA SILLA 3.6-M TELESCOPE.

Loral CCD (No. 40)		
Total area	$2048 \times 2048 \text{ pix}^2$	
Field of view	$5'.2 \times 5'.2$	
Pixel size	$15 \mu\text{m}$	
Image scale	$0''.16 \text{ pixel}^{-1}$	
Gain	$1.3 \text{ e}^- \text{ ADU}^{-1}$	
Read-noise (rms)	9 e^-	
Long slit		
Length	$\simeq 5'$	
Width	$1''.5$	
	Grating 7 ("blue")	Grating 11 ("low dispersion")
Groove density	600 lines mm^{-1}	300 lines mm^{-1}
Blaze λ (1st order)	3800 Å	4000 Å
Dispersion	$0.96 \text{ Å pixel}^{-1}$	$2.04 \text{ Å pixel}^{-1}$
Effective λ range	3270–5240 Å	3380–7520 Å

TABLE 3
LOG OF OBSERVATIONS.

H II Region (1)	Alternate Name(s) (2)	Date (UT 2003) (3)	Spectra (4)	N_{exp} (5)	t_{total} (s) (6)	$\langle X \rangle$ (7)	$ \Delta\theta $ ($^{\circ}$) (8)	[O III] $\lambda 4363$ (9)	RMS (mag) (10)
HK 16	...	26 Aug	Low disp.	3×1200	3600	1.11	8	...	0.030
HK 42	...	26 Aug	Low disp.	3×1200	3600	1.11	8	...	0.030
HK 69	...	28 Aug	Low disp.	3×1200	3600	1.03	20	...	0.034
HK 70	...	28 Aug	Low disp.	3×1200	3600	1.03	83	...	0.034
Hodge 7	KD 11	27 Aug	Low disp.	6×1200	7200	1.11	20	...	0.029
Hodge 12	KD 23	28 Aug	Low disp.	3×1200	3600	1.03	20	...	0.034
Hodge 12	KD 23	31 Aug	Blue	2×1200	2400	1.04	13	...	0.025
Hubble I	Hodge 2; KD 1	31 Aug	Blue	1×1200	1200	1.09	82	yes	0.025
Hubble III	Hodge 4; KD 4	31 Aug	Blue	1×1200	1200	1.09	82	...	0.025
Hubble V	Hodge 9, 11; KD 19	26 Aug	Low disp.	3×1200	3600	1.11	8	yes	0.030
Hubble V	Hodge 9, 11; KD 19	31 Aug	Blue	1×1200	1200	1.14	68	yes	0.025
K α	KD 2e	28 Aug	Low disp.	3×1200	3600	1.12	14	yes	0.034
K α	KD 2e	31 Aug	Blue	2×1200	2400	1.04	42	yes	0.025
K β	KD 5e	28 Aug ^a	Low disp.	3×1200	3600	1.12	14	...	0.034
K β	KD 5e	31 Aug ^b	Blue	2×1200	2400	1.04	42	yes	0.025
KD 9	...	26 Aug	Low disp.	3×1200	3600	1.11	8	...	0.030
KD 20	C10 ^c	28 Aug	Low disp.	3×1200	3600	1.09	83	...	0.034
KD 21	...	26 Aug	Low disp.	3×1200	3600	1.11	8	...	0.030
KD 22e	...	31 Aug	Blue	1×1200	1200	1.14	68	...	0.025
KD 24	...	28 Aug	Low disp.	3×1200	3600	1.03	20	...	0.034
KD 25	...	26 Aug	Low disp.	6×1200	7200	1.04	44	...	0.030
KD 28	...	27 Aug	Low disp.	6×1200	7200	1.07	54	...	0.029
KD 28e	...	28 Aug	Low disp.	3×1200	3600	1.09	83	yes	0.034
KD 28e	...	31 Aug	Blue	2×1200	2400	1.04	13	yes	0.025

NOTE. — Cols. (1) and (2): H II region, arranged in alphabetical order by their primary name and alternate names, respectively; see Hodge et al. (1988) for description. KD numbers followed by an “e” were identified as “stellar” objects in Table 3 of Killen & Dufour (1982). Col. (3): Date of observation. Col. (4): Spectra type; see Table 2. Col. (5): Number of exposures obtained and the length of each exposure in seconds. Col. (6): Total exposure time. Col. (7): Mean effective airmass. Col. (8): Average departure of the observing angle from the parallactic angle. Col. (9): [O III] $\lambda 4363$ detection. Col. (10): Relative root-mean-square error in the sensitivity function obtained from observations of standard stars.

^a The long-slit was placed through the center of the diffuse emission in K β .

^b The long-slit was placed through the bright feature to the northwest in K β .

^c The coordinates for KD 20 are the same for the object identified as “C10” by Chandar et al. (2000).

TABLE 4A
BLUE SPECTRA: LINE RATIOS AND PROPERTIES FOR NEBULAE HODGE 12, HUBBLE I, AND HUBBLE III.

Property	$f(\lambda)$	Ho 12		Hu I E ctr		Hu I NW spot	
		F	I	F	I	F	I
[O II] 3727	+0.325	341.2 ± 4.7	444.2 ± 6.1	222.6 ± 5.0	228.0 ± 6.2	235.4 ± 5.1	233.5 ± 5.1
[Ne III] 3869	+0.294	20.3 ± 1.9	25.8 ± 2.4	26.9 ± 3.9	27.5 ± 4.0	25.6 ± 3.9	25.4 ± 3.9
H8 + He I 3889	+0.289	22.5 ± 2.2	28.8 ± 2.8	19.8 ± 3.9	20.6 ± 4.0	16.3 ± 3.9	17.2 ± 3.9
Hε + He I 3970 ^a	+0.269	20.8 ± 2.2	26.6 ± 2.7	22.2 ± 3.9	23.0 ± 4.0	20.5 ± 4.0	21.0 ± 4.0
Hδ 4101	+0.232	18.6 ± 2.4	23.1 ± 2.9	27.1 ± 2.2	27.6 ± 2.3	29.0 ± 2.2	29.6 ± 2.2
Hγ 4340	+0.158	42.6 ± 1.6	48.7 ± 1.8	44.6 ± 2.2	45.3 ± 2.3	42.7 ± 1.7	43.0 ± 1.7
[O III] 4363	+0.151	5.2 ± 1.4	5.2 ± 1.4
Hβ 4861	0.000	100.0 ± 1.7	100.0 ± 1.7	100.0 ± 2.6	100.0 ± 2.6	100.0 ± 2.0	100.0 ± 2.0
[O III] 4959	-0.026	26.3 ± 1.4	25.6 ± 1.4	126.9 ± 3.0	126.4 ± 3.0	123.7 ± 6.3	122.7 ± 6.3
[O III] 5007	-0.038	76.8 ± 1.8	74.0 ± 1.7	378.1 ± 3.7	376.1 ± 3.7	368.6 ± 7.8	365.6 ± 7.7
$F(\text{H}\beta)$ (ergs s ⁻¹ cm ⁻²)		$(1.279 \pm 0.022) \times 10^{-15}$		$(9.28 \pm 0.24) \times 10^{-15}$		$(2.985 \pm 0.058) \times 10^{-15}$	
EW _e (Hβ) (Å)		350 ± 50		920 ± 500		242 ± 26	
Derived $E(B-V)$ (mag) ^b		+0.18 ± 0.16		+0.09 ± 0.20		+0.16 ± 0.17	
$c(\text{H}\beta)$		0.36		0.035		0	
Adopted A_V (mag)		+0.77		+0.07		0	
EW _{abs} (Å)		2		2		2	
Property	$f(\lambda)$	Hu III SE ring		Hu III NW arc		Hu III NW ring	
		F	I	F	I	F	I
[O II] 3727	+0.325	289.0 ± 7.0	347.0 ± 8.4	325.8 ± 9.8	366 ± 11	352.1 ± 7.6	323.4 ± 7.6
[Ne III] 3869	+0.294	27.9 ± 2.7	32.9 ± 3.2
H8 + He I 3889	+0.289	24.2 ± 2.3	30.1 ± 2.7
Hε + He I 3970 ^a	+0.269	18.0 ± 2.5	22.2 ± 2.9
Hδ 4101	+0.232	28.1 ± 2.1	32.7 ± 2.4	32.1 ± 3.1	34.9 ± 3.4	26.4 ± 2.4	26.8 ± 2.4
Hγ 4340	+0.158	42.3 ± 2.2	46.9 ± 2.4	44.0 ± 2.9	46.7 ± 3.1	50.5 ± 2.8	50.5 ± 2.8
Hβ 4861	0.000	100.0 ± 2.2	100.0 ± 2.2	100.0 ± 4.4	100.0 ± 4.4	100.0 ± 2.5	100.0 ± 2.5
[O III] 4959	-0.026	103.6 ± 2.1	101.6 ± 2.1	60.5 ± 4.2	59.7 ± 4.1	49.9 ± 2.1	49.6 ± 2.1
[O III] 5007	-0.038	299.6 ± 2.6	291.9 ± 2.5	190.1 ± 5.1	186.7 ± 5.0	144.9 ± 2.5	144.1 ± 2.5
$F(\text{H}\beta)$ (ergs s ⁻¹ cm ⁻²)		$(5.61 \pm 0.12) \times 10^{-15}$		$(1.817 \pm 0.080) \times 10^{-15}$		$(2.718 \pm 0.069) \times 10^{-15}$	
EW _e (Hβ) (Å)		470 ± 110		530 ± 300		375 ± 80	
Derived $E(B-V)$ (mag) ^b		+0.18 ± 0.19		+0.12 ± 0.26		-0.14 ± 0.21	
$c(\text{H}\beta)$		0.25		0.16		0	
Adopted A_V (mag)		+0.53		+0.34		0	
EW _{abs} (Å)		2		2		2	

NOTE. — Emission lines are listed in Å. F is the observed flux ratio with respect to Hβ. I is the corrected intensity ratio, corrected for the adopted reddening listed, and for underlying Balmer absorption. The uncertainties in the observed line ratios account for the uncertainties in the fits to the line profiles, the surrounding continua, and the relative uncertainty in the sensitivity function listed in Table 3. Flux uncertainties in the Hβ reference line are not included. Uncertainties in the corrected line ratios account for uncertainties in the specified line and in the Hβ reference line. The reddening function, $f(\lambda)$, is given. Also listed are the observed Hβ flux; the equivalent width of Hβ in emission, EW_e(Hβ). Where [O III] λ4363 is measured, simultaneous solutions for the logarithmic reddening, $c(\text{H}\beta)$, and the equivalent width of the underlying Balmer absorption, EW_{abs} are listed. The adopted value of the extinction in V, A_V , is listed. Where [O III] λ4363 is not measured, the equivalent width of the underlying Balmer absorption was set to 2 Å.

^a Blended with [Ne III] λ 3967.

^b Derived from $F(\text{H}\gamma)/F(\text{H}\beta)$.

TABLE 4B
BLUE SPECTRA: LINE RATIOS AND PROPERTIES FOR NEBULAE HUBBLE V, K α , K β , KD 22E, AND KD 28E.

Property	$f(\lambda)$	Hu V		K α		K β	
		F	I	F	I	F	I
[O II] 3727	+0.325	115.98 \pm 0.91	141.0 \pm 1.1	79.95 \pm 0.94	97.9 \pm 1.2	154.8 \pm 2.2	202.2 \pm 2.9
H12 3751	+0.320	1.84 \pm 0.70	2.79 \pm 0.85	1.6 \pm 1.7	2.4 \pm 2.2
H11 3772	+0.316	2.62 \pm 0.72	3.84 \pm 0.87	1.89 \pm 0.71	3.16 \pm 0.86	2.4 \pm 1.7	3.4 \pm 2.2
H10 3799	+0.310	4.14 \pm 0.76	5.83 \pm 0.91	3.30 \pm 0.75	5.07 \pm 0.91	3.8 \pm 1.8	5.2 \pm 2.3
H9 3835	+0.302	5.09 \pm 0.63	7.15 \pm 0.75	5.83 \pm 0.65	8.21 \pm 0.78	7.9 \pm 1.3	10.5 \pm 1.7
[Ne III] 3869	+0.294	30.81 \pm 0.74	36.73 \pm 0.88	39.93 \pm 0.76	47.93 \pm 0.91	35.5 \pm 1.4	45.2 \pm 1.8
H8+He I 3889	+0.289	14.85 \pm 0.65	18.91 \pm 0.77	15.00 \pm 0.65	19.35 \pm 0.78	18.4 \pm 1.2	23.8 \pm 1.5
He+He I 3970 ^a	+0.269	21.00 \pm 0.36	25.87 \pm 0.42	21.87 \pm 0.37	27.17 \pm 0.44	20.4 \pm 1.3	25.9 \pm 1.6
He I 4027	+0.253	1.64 \pm 0.31	1.91 \pm 0.36	1.35 \pm 0.30	1.58 \pm 0.35	1.21 \pm 0.48	1.49 \pm 0.59
[S II] 4068, 4076	+0.241	1.02 \pm 0.32	1.18 \pm 0.37	0.64 \pm 0.35	0.74 \pm 0.41	1.32 \pm 0.46	1.61 \pm 0.56
H δ 4101	+0.232	21.70 \pm 0.37	26.05 \pm 0.42	21.88 \pm 0.44	26.45 \pm 0.51	21.27 \pm 0.58	26.10 \pm 0.70
H γ 4340	+0.158	41.63 \pm 0.78	46.53 \pm 0.85	40.9 \pm 1.0	46.0 \pm 1.1	40.6 \pm 1.3	46.5 \pm 1.5
[O III] 4363	+0.151	5.22 \pm 0.60	5.69 \pm 0.65	6.75 \pm 0.81	7.39 \pm 0.89	4.9 \pm 1.0	5.5 \pm 1.1
He I 4388	+0.143	0.47 \pm 0.60	0.51 \pm 0.65
He I 4471	+0.116	3.48 \pm 0.11	3.71 \pm 0.12	2.84 \pm 0.23	3.04 \pm 0.25	3.55 \pm 0.48	3.90 \pm 0.53
[Ar IV]+He I 4713	+0.042	0.61 \pm 0.07	0.62 \pm 0.07
H β 4861	0.000	100.0 \pm 1.3	100.0 \pm 1.3	100.0 \pm 1.0	100.00 \pm 0.99	100.0 \pm 1.2	100.0 \pm 1.2
He I 4922	-0.016	0.97 \pm 0.09	0.95 \pm 0.08	2.1 \pm 3.7	2.1 \pm 3.6
[O III] 4959	-0.026	179.7 \pm 4.3	175.6 \pm 4.2	198.3 \pm 3.7	193.7 \pm 3.6	177.7 \pm 3.3	173.5 \pm 3.2
[O III] 5007	-0.038	534.8 \pm 5.3	518.6 \pm 5.1	592.8 \pm 4.5	574.4 \pm 4.4	533.8 \pm 3.9	515.8 \pm 3.8
$F(\text{H}\beta)$ (ergs s ⁻¹ cm ⁻²)		(9.48 \pm 0.12) $\times 10^{-14}$		(1.328 \pm 0.014) $\times 10^{-14}$		(6.438 \pm 0.079) $\times 10^{-15}$	
EW _e (H β) (Å)		239 \pm 18		261 \pm 18		507 \pm 77	
Derived $E(B-V)$ (mag) ^b		+0.20 \pm 0.14		+0.23 \pm 0.14		+0.26 \pm 0.15	
$c(\text{H}\beta)$		0.27		0.28		0.36	
Adopted A_V (mag)		+0.57		+0.60		+0.77	
EW _{abs} (Å)		1.7		1.8		1.3	
Property	$f(\lambda)$	KD 22e		KD 28e			
		F	I	F	I		
[O II] 3727	+0.325	478.2 \pm 6.8	472.8 \pm 6.7	218.6 \pm 1.9	239.6 \pm 2.1		
H12 3751	+0.320	1.7 \pm 1.5	2.3 \pm 1.6		
H11 3772	+0.316	5.3 \pm 1.5	6.2 \pm 1.6		
H10 3799	+0.310	6.3 \pm 1.6	7.4 \pm 1.8		
H9 3835	+0.302	6.32 \pm 0.76	7.74 \pm 0.83		
[Ne III] 3869	+0.294	26.97 \pm 0.88	29.29 \pm 0.96		
H8+He I 3889	+0.289	17.59 \pm 0.82	20.01 \pm 0.89		
He+He I 3970 ^a	+0.269	21.15 \pm 0.61	23.72 \pm 0.66		
H δ 4101	+0.232	24.2 \pm 3.4	26.3 \pm 3.4	23.43 \pm 0.62	25.85 \pm 0.66		
H γ 4340	+0.158	51.0 \pm 2.1	52.2 \pm 2.1	44.34 \pm 0.74	46.88 \pm 0.77		
[O III] 4363	+0.151	3.99 \pm 0.59	4.15 \pm 0.61		
He I 4471	+0.116	2.74 \pm 0.29	2.82 \pm 0.30		
H β 4861	0.000	100.0 \pm 2.6	100.0 \pm 2.6	100.00 \pm 0.79	100.00 \pm 0.79		
[O III] 4959	-0.026	28.7 \pm 2.2	28.4 \pm 2.2	141.8 \pm 1.8	139.9 \pm 1.8		
[O III] 5007	-0.038	68.9 \pm 2.4	68.1 \pm 2.4	424.3 \pm 2.2	417.2 \pm 2.2		
$F(\text{H}\beta)$ (ergs s ⁻¹ cm ⁻²)		(3.347 \pm 0.086) $\times 10^{-15}$		(4.276 \pm 0.034) $\times 10^{-15}$			
EW _e (H β) (Å)		174 \pm 18		396 \pm 32			
Derived $E(B-V)$ (mag) ^b		0		+0.09 \pm 0.13			
$c(\text{H}\beta)$		0		0.13			
Adopted A_V (mag)		0		+0.28			
EW _{abs} (Å)		2		2.2			

NOTE. — See Table 4a for additional comments.

^a Blended with [Ne III] λ 3967.

^b Derived from $F(\text{H}\gamma)/F(\text{H}\beta)$.

TABLE 5A
LOW-DISPERSION SPECTRA: LINE RATIOS AND PROPERTIES FOR NEBULAE HK 16, HK 42, HK 69, HK 70, HODGE 7, AND HODGE 12.

Property	$f(\lambda)$	HK 16		HK 42		HK 69	
		F	I	F	I	F	I
[O II] 3727	+0.325	399 ± 26	496 ± 32	391 ± 38	559 ± 54	424 ± 19	
H β 4861	0.000	100 ± 14	100 ± 13	100 ± 13	100 ± 12	100 ± 11	
[O III] 4959	-0.026	6 ± 10	6 ± 10	126 ± 16	112 ± 14	...	
[O III] 5007	-0.038	62 ± 11	59 ± 10	353 ± 21	308 ± 18	...	
H α 6563	-0.299	363 ± 16	285 ± 12	460 ± 24	286 ± 15	504 ± 18	
[N II] 6583	-0.301	44 ± 13	35 ± 10	17 ± 19	10 ± 12	14 ± 15	
[S II] 6716	-0.319	91 ± 12	70.3 ± 9.1	10 ± 18	6 ± 10	132 ± 13 ^a	
[S II] 6731	-0.321	41 ± 12	31.6 ± 9.3	31 ± 18	19 ± 11	132 ± 13 ^a	
$F(\text{H}\beta)$ (ergs s ⁻¹ cm ⁻²)		$(1.06 \pm 0.15) \times 10^{-16}$		$(6.88 \pm 0.93) \times 10^{-17}$		$(1.66 \pm 0.18) \times 10^{-16}$	
EW _e (H β) (Å)		85 ± 19		23.2 ± 3.5		... ^b	
Derived $E(B-V)$ (mag) ^c		+0.22 ± 0.20		+0.41 ± 0.22		+0.57 ± 0.16	
$c(\text{H}\beta)$		0.32		0.59		...	
Adopted A_V (mag)		+0.68		+1.25		+1.74	
EW _{abs} (Å)		2		2		...	
Property	$f(\lambda)$	HK 70		Ho 7		Ho 12	
		F	I	F	I	F	I
[O II] 3727	+0.325	311 ± 25	488 ± 39	290.2 ± 9.5	474 ± 130	362.4 ± 7.3	535 ± 24
[Ne III] 3869	+0.294	60 ± 10	90 ± 15	19.7 ± 2.1	28.0 ± 3.2
H8 + He I 3889	+0.289	18.8 ± 2.9	28.0 ± 4.2
He + He I 3970 ^d	+0.269	17.7 ± 1.7	26.2 ± 2.5
[S II] 4068, 4076	+0.241	16.3 ± 1.8	21.7 ± 2.5
H δ 4101	+0.232	33.7 ± 9.8	46 ± 14	19.8 ± 1.9	27.4 ± 2.6
H γ 4340	+0.158	48.8 ± 8.5	61 ± 11	27.4 ± 2.8	33.3 ± 8.2	40.8 ± 2.0	50.3 ± 2.6
[O III] 4363	+0.151	5.4 ± 1.6	6.4 ± 1.9
H β 4861	0.000	100 ± 12	100 ± 12	100.0 ± 6.0	100.0 ± 6.9	100.0 ± 3.7	100.0 ± 3.7
[O III] 4959	-0.026	152 ± 13	147 ± 13	72.5 ± 6.3	71 ± 11	21.1 ± 1.6	20.3 ± 1.5
[O III] 5007	-0.038	463 ± 17	440 ± 16	203.8 ± 8.2	197 ± 21	59.8 ± 2.0	56.6 ± 1.9
He I 5876	-0.204	10.5 ± 1.6	8.1 ± 1.3
[O I] 6300 + [S III] 6312	-0.264	73.6 ± 4.8	52.8 ± 3.8
[O I] 6363	-0.272	27.0 ± 2.1	19.2 ± 1.6
H α 6563	-0.299	442 ± 15	292.0 ± 9.7	403 ± 13	286 ± 88	411.9 ± 9.3	284 ± 12
[N II] 6583	-0.301	33 ± 12	21.7 ± 8.0	4 ± 11	3 ± 8	38.8 ± 7.8	26.6 ± 5.4
[S II] 6716	-0.319	86 ± 11	55.5 ± 7.3	226.2 ± 5.3 ^a	151.7 ± 6.9
[S II] 6731	-0.321	52 ± 12	33.4 ± 7.4	226.2 ± 5.3 ^a	151.7 ± 6.9
He I 7281	-0.395	34.5 ± 4.1	21.1 ± 2.7
[O II] 7320, 7330	-0.400	46.1 ± 4.4	28.0 ± 3.0
$F(\text{H}\beta)$ (ergs s ⁻¹ cm ⁻²)		$(1.36 \pm 0.17) \times 10^{-16}$		$(1.233 \pm 0.074) \times 10^{-16}$		$(1.084 \pm 0.040) \times 10^{-15}$	
EW _e (H β) (Å)		74 ± 15		... ^b		148 ± 16	
Derived $E(B-V)$ (mag) ^c		+0.42 ± 0.18		+0.35 ± 0.11		+0.359 ± 0.089	
$c(\text{H}\beta)$		0.60		...		0.530 ± 0.053	
Adopted A_V (mag)		+1.29		+1.07		+1.13	
EW _{abs} (Å)		0		2		1.3	

NOTE. — See Table 4a for additional comments.

^a [S II] unresolved.

^b Very weak continuum.

^c Derived from $F(\text{H}\alpha)/F(\text{H}\beta)$.

^d Blended with [Ne III] λ 3967.

TABLE 5B
LOW-DISPERSION SPECTRA: LINE RATIOS AND PROPERTIES FOR NEBULAE HUBBLE V, K α , K β , KD 9, KD 20, AND KD 21.

		Hu V		K α		K β	
Property	$f(\lambda)$	F	I	F	I	F	I
[O II] 3727	+0.325	90.2 \pm 1.6	128.9 \pm 6.4	76.9 \pm 1.5	125.4 \pm 5.2	404 \pm 24	574 \pm 84
H12 3751	+0.320	1.2 \pm 1.1	1.9 \pm 1.8
H11 3772	+0.316	2.0 \pm 1.2	2.8 \pm 1.7	2.6 \pm 1.1	4.2 \pm 1.8
H10 3799	+0.310	3.3 \pm 1.3	4.6 \pm 1.8	4.8 \pm 1.2	7.7 \pm 1.9
H9 3835	+0.302	5.57 \pm 0.71	7.8 \pm 1.0	4.74 \pm 0.80	7.5 \pm 1.3
[Ne III] 3869	+0.294	35.14 \pm 0.75	48.5 \pm 2.3	39.19 \pm 0.93	61.0 \pm 2.5
H8 + He I 3889	+0.289	14.88 \pm 0.65	20.4 \pm 1.2	14.11 \pm 0.80	21.8 \pm 1.4
He ϵ + He I 3970 ^a	+0.269	23.63 \pm 0.50	31.8 \pm 1.4	20.83 \pm 0.60	31.2 \pm 1.3
He I 4027	+0.253	1.36 \pm 0.36	1.80 \pm 0.48	1.05 \pm 0.49	1.54 \pm 0.72
[S II] 4068, 4076	+0.241	0.91 \pm 0.49	1.19 \pm 0.64	0.61 \pm 0.48	0.88 \pm 0.69
H δ 4101	+0.232	21.44 \pm 0.58	27.7 \pm 1.2	20.78 \pm 0.57	29.4 \pm 1.1
H γ 4340	+0.158	40.59 \pm 0.98	48.3 \pm 1.6	40.37 \pm 0.98	51.2 \pm 1.5	40.4 \pm 6.4	47 \pm 12
[O III] 4363	+0.151	5.05 \pm 0.72	5.96 \pm 0.86	7.47 \pm 0.78	9.37 \pm 0.99
He I 4388	+0.143	0.54 \pm 0.74	0.63 \pm 0.87
He I 4471	+0.116	3.62 \pm 0.14	4.11 \pm 0.17	3.80 \pm 0.21	4.53 \pm 0.26
[Ar IV] + He I 4713	+0.042	0.645 \pm 0.070	0.68 \pm 0.07	0.99 \pm 0.15	1.05 \pm 0.16
[Ar IV] 4740	+0.034	0.214 \pm 0.054	0.22 \pm 0.06
H β 4861	0.000	100.0 \pm 3.8	100.0 \pm 3.8	100.0 \pm 2.7	100.0 \pm 2.7	100.0 \pm 7.4	100.0 \pm 8.1
He I 4922	-0.016	1.06 \pm 0.12	1.04 \pm 0.12	1.2 \pm 2.3	1.2 \pm 2.2
[O III] 4959	-0.026	195 \pm 14	189 \pm 13	197 \pm 13	189 \pm 12	18.0 \pm 5.9	17.7 \pm 7.3
[O III] 5007	-0.038	572 \pm 18	549 \pm 18	596 \pm 17	563 \pm 16	70.2 \pm 7.0	68 \pm 13
[N I] 5199	-0.083	0.160 \pm 0.043	0.15 \pm 0.04	0.47 \pm 0.11	0.41 \pm 0.10
He I 5876	-0.204	14.16 \pm 0.51	11.31 \pm 0.52	16.15 \pm 0.58	11.87 \pm 0.51
[O I] 6300	-0.264	0.11 \pm 0.33	0.08 \pm 0.25	3.19 \pm 0.30	2.14 \pm 0.21
[S III] 6312	-0.266	3.58 \pm 0.33	2.67 \pm 0.26	1.33 \pm 0.27	0.89 \pm 0.18
[O I] 6363	-0.272	0.58 \pm 0.13	0.43 \pm 0.10	0.85 \pm 0.27	0.56 \pm 0.18
H α 6563	-0.299	405 \pm 10	291 \pm 14	457 \pm 10	291 \pm 12	369 \pm 12	286 \pm 36
[N II] 6583	-0.301	1.98 \pm 0.12	1.42 \pm 0.11	3.74 \pm 0.46	2.37 \pm 0.30	8 \pm 10	6.3 \pm 8.6
He I 6678	-0.314	4.75 \pm 0.34	3.36 \pm 0.28	5.39 \pm 0.28	3.36 \pm 0.21
[S II] 6716	-0.319	8.36 \pm 0.42	5.88 \pm 0.40	8.17 \pm 0.28	5.05 \pm 0.25	51.6 \pm 8.6 ^b	39.5 \pm 9.9
[S II] 6731	-0.321	6.18 \pm 0.38	4.34 \pm 0.33	7.09 \pm 0.27	4.37 \pm 0.23	51.6 \pm 8.6 ^b	39.5 \pm 9.9
He I 7065	-0.366	4.10 \pm 0.18	2.74 \pm 0.19	12.01 \pm 0.24	6.92 \pm 0.32
[Ar III] 7136	-0.375	14.91 \pm 0.23	9.87 \pm 0.55	18.75 \pm 0.26	10.7 \pm 0.47
He I 7281	-0.395	1.011 \pm 0.082	0.66 \pm 0.06	1.70 \pm 0.18	0.94 \pm 0.11
[O II] 7320	-0.400	4.61 \pm 0.10 ^c	2.97 \pm 0.18	5.98 \pm 0.27	3.28 \pm 0.21
[O II] 7330	-0.402	4.61 \pm 0.10 ^c	2.97 \pm 0.18	4.43 \pm 0.25	2.42 \pm 0.17
$F(\text{H}\beta)$ (ergs s ⁻¹ cm ⁻²)		(3.15 \pm 0.12) $\times 10^{-14}$		(6.31 \pm 0.17) $\times 10^{-15}$		(1.90 \pm 0.14) $\times 10^{-16}$	
EW _c (H β) (Å)		288 \pm 58		207 \pm 25		... ^d	
Derived $E(B - V)$ (mag) ^e		+0.34 \pm 0.10		+0.466 \pm 0.081		+0.26 \pm 0.13	
$c(\text{H}\beta)$		0.477 \pm 0.061		0.653 \pm 0.049		...	
Adopted A_V (mag)		+1.01		+1.39		+0.80	
EW _{abs} (Å)		0		0		2	
		KD 9		KD 20		KD 21	
Property	$f(\lambda)$	F	I	F		F	I
[O II] 3727	+0.325	311 \pm 29	377 \pm 35	789 \pm 65		335.8 \pm 7.4	427 \pm 25
H δ 4101	+0.232		17.2 \pm 2.0	25.1 \pm 2.6
H γ 4340	+0.158		44.2 \pm 2.8	52.4 \pm 3.4
H β 4861	0.000	100 \pm 14	100 \pm 14	100 \pm 23		100.0 \pm 4.2	100.0 \pm 4.1
[O III] 4959	-0.026	50 \pm 11	48 \pm 11	...		43.0 \pm 3.4	40.8 \pm 3.2
[O III] 5007	-0.038	87 \pm 14	83 \pm 13	...		112.8 \pm 4.2	106.0 \pm 4.0
He I 5876	-0.204		10.6 \pm 1.7	8.7 \pm 1.4
H α 6563	-0.299	353 \pm 23	286 \pm 18	536 \pm 34		393.0 \pm 7.9	298 \pm 16
[N II] 6583	-0.301	10 \pm 20	8 \pm 16	10 \pm 28		10.1 \pm 6.5	7.6 \pm 4.9
[S II] 6716	-0.319	27 \pm 17	22 \pm 13	226 \pm 28 ^b		48.4 \pm 5.9	35.9 \pm 4.8
[S II] 6731	-0.321	36 \pm 17	28 \pm 13	226 \pm 28 ^b		28.6 \pm 6.0	21.2 \pm 4.6
$F(\text{H}\beta)$ (ergs s ⁻¹ cm ⁻²)		(5.57 \pm 0.77) $\times 10^{-17}$		(5.2 \pm 1.2) $\times 10^{-17}$		(6.40 \pm 0.27) $\times 10^{-16}$	
EW _c (H β) (Å)		78 \pm 18		... ^d		65.0 \pm 4.0	
Derived $E(B - V)$ (mag) ^e		+0.20 \pm 0.23		+0.65 \pm 0.33		+0.295 \pm 0.092	
$c(\text{H}\beta)$		0.29		...		0.363 \pm 0.072	
Adopted A_V (mag)		+0.62		+2.0		+0.77	
EW _{abs} (Å)		2		2		2	

NOTE. — See Table 4a for additional comments.

^a Blended with [Ne III] λ 3967.

^b [S II] unresolved.

^c [O II] $\lambda\lambda$ 7320, 7330 unresolved.

^d Very weak continuum.

^e Derived from $F(\text{H}\alpha)/F(\text{H}\beta)$.

TABLE 5c
LOW-DISPERSION SPECTRA: LINE RATIOS AND PROPERTIES FOR NEBULAE KD 24, KD 25, KD 28, AND KD 28e.

Property	$f(\lambda)$	KD 24		KD 25		KD 28	
		F	I	F	I	F	I
[O II] 3727	+0.325	377 ± 14	813 ± 90	371 ± 11	539 ± 17	315 ± 19	468 ± 28
H γ 4340	+0.158	42.6 ± 4.4	55.8 ± 9.8	32.7 ± 6.3	42.1 ± 7.5	40.9 ± 7.4	52.6 ± 8.9
H β 4861	0.000	100.0 ± 4.5	100.0 ± 6.2	100.0 ± 5.4	100.0 ± 5.3	100.0 ± 8.8	100.0 ± 8.6
[O III] 4959	-0.026	7.2 ± 3.3	6.9 ± 3.6	16.8 ± 4.1	15.9 ± 3.9	19.9 ± 7.1	18.8 ± 6.7
[O III] 5007	-0.038	19.3 ± 3.5	18.1 ± 4.5	35.8 ± 4.5	33.3 ± 4.2	78.6 ± 8.5	73.2 ± 7.9
H α 6563	-0.299	496 ± 11	286 ± 29	416.9 ± 9.3	283.9 ± 6.3	432 ± 19	288 ± 12
[N II] 6583	-0.301	26.1 ± 9.6	15.0 ± 6.5	9.5 ± 7.8	6.4 ± 5.3	3 ± 15	3 ± 12
[S II] 6716, 6731	-0.320	120.9 ± 8.4	67.5 ± 9.4	72.3 ± 6.7	47.7 ± 4.4	77 ± 13	49.9 ± 8.7
$F(\text{H}\beta)$ (ergs s $^{-1}$ cm $^{-2}$)		$(6.77 \pm 0.30) \times 10^{-16}$		$(1.243 \pm 0.067) \times 10^{-16}$		$(4.89 \pm 0.43) \times 10^{-17}$	
EW $_{\text{e}}(\text{H}\beta)$ (Å)		... ^a		81.2 ± 7.0		93 ± 15	
Derived $E(B-V)$ (mag) ^b		$+0.56 \pm 0.10$		$+0.36 \pm 0.10$		$+0.40 \pm 0.15$	
$c(\text{H}\beta)$...		0.53		0.56	
Adopted A_V (mag)		$+1.72$		$+1.13$		$+1.19$	
EW $_{\text{abs}}$ (Å)		2		2		2	
KD 28e							
Property	$f(\lambda)$	F	I				
[O II] 3727	+0.325	229.2 ± 3.1	305.3 ± 9.6				
H11 3772	+0.316	3.4 ± 2.4	4.5 ± 3.2				
H10 3799	+0.310	4.8 ± 2.6	6.3 ± 3.4				
H9 3835	+0.302	6.41 ± 0.60	8.36 ± 0.81				
[Ne III] 3869	+0.294	27.46 ± 0.62	35.6 ± 1.2				
H8+He I 3889	+0.289	17.96 ± 0.59	23.17 ± 0.96				
He+He I 3970 ^c	+0.269	20.96 ± 0.62	26.6 ± 1.0				
[S II] 4068, 4076	+0.241	1.45 ± 0.46	1.79 ± 0.57				
H δ 4101	+0.232	22.67 ± 0.59	27.81 ± 0.92				
H γ 4340	+0.158	42.42 ± 0.66	48.8 ± 1.0				
[O III] 4363	+0.151	3.49 ± 0.52	3.99 ± 0.60				
He I 4471	+0.116	3.86 ± 0.34	4.28 ± 0.38				
H β 4861	0.000	100.0 ± 2.5	100.0 ± 2.5				
[O III] 4959	-0.026	138.0 ± 6.3	134.9 ± 6.2				
[O III] 5007	-0.038	412.4 ± 8.1	398.7 ± 7.9				
He I 5876	-0.204	12.93 ± 0.47	10.80 ± 0.44				
[O I] 6300+[S III] 6312	-0.264	3.75 ± 0.46	2.97 ± 0.37				
[O I] 6363	-0.272	1.14 ± 0.36	0.90 ± 0.28				
H α 6563	-0.299	377.7 ± 4.9	290.1 ± 8.5				
[N II] 6583	-0.301	9.4 ± 1.4	7.2 ± 1.1				
He I 6678	-0.314	3.8 ± 3.7	2.9 ± 2.8				
[S II] 6716	-0.319	16.7 ± 3.8	12.6 ± 2.9				
[S II] 6731	-0.321	12.9 ± 3.9	9.7 ± 3.0				
He I 7065	-0.366	4.18 ± 0.42	3.03 ± 0.32				
[Ar III] 7136	-0.375	17.33 ± 0.49	12.44 ± 0.54				
He I 7281	-0.395	1.46 ± 0.40	1.03 ± 0.28				
[O II] 7320	-0.400	6.63 ± 0.49	4.66 ± 0.38				
[O II] 7330	-0.401	3.62 ± 0.49	2.54 ± 0.36				
$F(\text{H}\beta)$ (ergs s $^{-1}$ cm $^{-2}$)		$(3.782 \pm 0.094) \times 10^{-15}$					
EW $_{\text{e}}(\text{H}\beta)$ (Å)		337 \pm 56					
Derived $E(B-V)$ (mag) ^b		$+0.277 \pm 0.074$					
$c(\text{H}\beta)$		0.383 ± 0.039					
Adopted A_V (mag)		$+0.81$					
EW $_{\text{abs}}$ (Å)		0					

NOTE. — See Table 4a for additional comments.

^a Very weak continuum.

^b Derived from $F(\text{H}\alpha)/F(\text{H}\beta)$.

^c Blended with [Ne III] λ 3967.

a

TABLE 6A
IONIC AND TOTAL ABUNDANCES.

Property	HK 16	HK 42	HK 69	HK 70	Ho 7	Ho 12	Ho 12	Hu I	Hu I	Hu III
	Low disp.	Low disp.	Low disp.	Low disp.	Low disp.	Blue	Low disp.	E ctr ^a	NW spot ^a	SE ring ^a
$T_e(\text{O}^{+2})$ (K)	13100 ± 1500	...
$T_e(\text{O}^+)$ (K) ^b	12200 ± 1400	...
$\text{O}^+/\text{H} (\times 10^5)$	3.9 ± 1.6	...
$\text{O}^{+2}/\text{H} (\times 10^5)$	5.5 ± 1.6	...
$\text{O}/\text{H} (\times 10^5)$	9.4 ± 2.3	...
$12+\log(\text{O}/\text{H})$	$> 8.10^c$	$7.98 \pm 0.09^{(+0.11)}_{(-0.15)}$...
$12+\log(\text{O}/\text{H})$ M91 ^d	8.28	... ^e ^e	8.26	8.18	8.32	8.05	8.05	8.16
$12+\log(\text{O}/\text{H})$ P00 ^f	...	8.43	...	8.30	8.38	7.88	7.89	8.09
$\text{Ne}^{+2}/\text{O}^{+2}$	0.23 ± 0.10	...
$\log(\text{Ne}/\text{O})$	-0.64 ± 0.19	...

NOTE. — Nebulae are listed in the same order as they appear in Table 3. Direct oxygen abundances are shown with two uncertainties. The first uncertainty is the formal uncertainty in the derivation. In parentheses is the range of possible values, expressed by the maximum and minimum values of the oxygen abundance.

^a See Fig. 2 for locations of resolved features.

^b O^+ zone temperature derived using Equation 1; see Campbell et al. (1986) and Garnett (1992).

^c Lower limit to the oxygen abundance, as $[\text{O III}] \lambda\lambda 4959, 5007$ was not detected.

^d McGaugh (1991) bright-line calibration.

^e $\log R_{23} \gtrsim 1$.

^f Pilyugin (2000) bright-line calibration.

b

TABLE 6B
IONIC AND TOTAL ABUNDANCES (CONTINUED).

Property	Hu III NW arc ^a	Hu III NW ring ^a	Hu V	Hu V	K α	K α	K β	K β
	Blue	Blue	Blue	Low disp.	Blue	Low disp.	Blue	Low disp.
$T_e(\text{O}^{+2})$ (K)	11930 ± 500	11860 ± 640	12660 ± 590	14060 ± 660	11840 ± 900	...
$T_e(\text{O}^+)$ (K) ^b	11350 ± 500	11300 ± 610	11860 ± 560	12840 ± 610	11290 ± 860	...
$T_e(\text{O}^+)$ (K) ^c	11200 ± 750	...	15900 ± 1600
$T_e(\text{S}^+)$ (K) ^d	13000 ± 10000	...	9800 ± 9200
$\text{O}^+/\text{H} (\times 10^5)$	3.11 ± 0.52	2.90 ± 0.61	1.83 ± 0.31	1.76 ± 0.29	4.6 ± 1.3	...
$\text{O}^{+2}/\text{H} (\times 10^5)$	10.3 ± 1.2	11.1 ± 1.7	9.6 ± 1.2	7.06 ± 0.83	10.4 ± 2.2	...
$\text{O}/\text{H} (\times 10^5)$	13.4 ± 1.3	13.9 ± 1.8	11.4 ± 1.2	8.83 ± 0.88	15.0 ± 2.6	...
$12+\log(\text{O}/\text{H})$	$8.13 \pm 0.04^{(+0.05)}_{(-0.06)}$	$8.15 \pm 0.05^{(+0.06)}_{(-0.07)}$	$8.06 \pm 0.04^{(+0.05)}_{(-0.06)}$	$7.95 \pm 0.04^{(+0.05)}_{(-0.06)}$	$8.18 \pm 0.07^{(+0.09)}_{(-0.11)}$...
$12+\log(\text{O}/\text{H})$ M91 ^e	8.09	7.99	8.06	8.07	8.03	8.07	8.16	8.37
$12+\log(\text{O}/\text{H})$ P00 ^f	8.18	8.13	7.83	7.83	7.80	7.83	7.92	...
$\text{Ar}^{+2}/\text{H} (\times 10^7)$	6.48 ± 0.98	...	5.28 ± 0.29
$\text{Ar}^{+3}/\text{H} (\times 10^7)$	0.29 ± 0.13
$\text{ICF}(\text{Ar})$	1.05	...	1.80
$\text{Ar}/\text{H} (\times 10^7)$	7.1 ± 1.2	...	9.5 ± 1.1
$\log(\text{Ar}/\text{O})$	-2.29 ± 0.04	...	-1.96 ± 0.03
$\text{N}^+/\text{O}^+ (\times 10^2)$	0.703 ± 0.067	...	1.44 ± 0.20
$\log(\text{N}/\text{O})$	-2.15 ± 0.04	...	-1.84 ± 0.06
$\text{Ne}^{+2}/\text{O}^{+2}$	0.208 ± 0.053	0.267 ± 0.062	0.245 ± 0.063	0.324 ± 0.067	0.261 ± 0.080	...
$\log(\text{Ne}/\text{O})$	-0.68 ± 0.11	-0.57 ± 0.10	-0.61 ± 0.11	-0.489 ± 0.091	-0.58 ± 0.13	...

NOTE. — See Table 6a for additional comments.

^a See Fig. 2 for locations of resolved features.

^b O^+ zone temperature derived using Equation 1; see Campbell et al. (1986) and Garnett (1992).

^c O^+ zone temperature derived from $I([\text{O II}] \lambda 3727)/I([\text{O II}] \lambda \lambda 7320, 7330)$.

^d S^+ zone temperature derived from $I([\text{S II}] \lambda \lambda 6716, 6731)/I([\text{S II}] \lambda \lambda 4068, 4076)$.

^e McGaugh (1991) bright-line calibration.

^f Pilyugin (2000) bright-line calibration.

TABLE 6C
IONIC AND TOTAL ABUNDANCES (CONTINUED).

Property	KD 9 Low disp.	KD 20 Low disp.	KD 21 Low disp.	KD 22e Blue	KD 24 Low disp.	KD 25 Low disp.	KD 28 Low disp.	KD 28e Blue	KD 28e Low disp.
$T_e(\text{O}^{+2})$ (K)	11530 ± 610	11540 ± 620
$T_e(\text{O}^+)$ (K) ^a	11070 ± 580	11080 ± 600
$T_e(\text{O}^+)$ (K) ^b	11180 ± 720
$T_e(\text{S}^+)$ (K) ^c	9500 ± 4100
O^+/H ($\times 10^5$)	5.8 ± 1.2	7.4 ± 1.6
O^{+2}/H ($\times 10^5$)	9.2 ± 1.4	8.7 ± 1.4
O/H ($\times 10^5$)	$> 8.13^{\text{d}}$	15.0 ± 1.8	16.2 ± 2.1
$12+\log(\text{O}/\text{H})$	$8.18 \pm 0.05^{(+0.06)}_{(-0.07)}$	$8.21 \pm 0.05^{(+0.06)}_{(-0.07)}$
$12+\log(\text{O}/\text{H})$ M91 ^e	8.06	...	8.15	8.22	...	8.37	8.22	8.12	8.20
$12+\log(\text{O}/\text{H})$ P00 ^f	8.40	...	8.48	7.93	8.03
Ar^{+2}/H ($\times 10^7$)	8.6 ± 1.1
ICF(Ar)	1.45
Ar/H ($\times 10^7$)	12.5 ± 1.6
$\log(\text{Ar}/\text{O})$	-2.11 ± 0.04
N^+/O^+ ($\times 10^2$)	1.46 ± 0.23
$\log(\text{N}/\text{O})$	-1.83 ± 0.06
$\text{Ne}^{+2}/\text{O}^{+2}$	0.204 ± 0.053	0.271 ± 0.053
$\log(\text{Ne}/\text{O})$	-0.68 ± 0.11	-0.567 ± 0.086

NOTE. — See Table 6a for additional comments.

^a O^+ zone temperature derived using Equation 1; see Campbell et al. (1986) and Garnett (1992).

^b O^+ zone temperature derived from $I([\text{O II}] \lambda 3727)/I([\text{O II}] \lambda \lambda 7320, 7330)$.

^c S^+ zone temperature derived from $I([\text{S II}] \lambda \lambda 6716, 6731)/I([\text{S II}] \lambda \lambda 4068, 4076)$.

^d Lower limit to the oxygen abundance, as $[\text{O III}] \lambda \lambda 4959, 5007$ was barely detected.

^e McGaugh (1991) bright-line calibration.

^f Pilyugin (2000) bright-line calibration.

TABLE 7
OXYGEN ABUNDANCES IN NGC 6822.

Object	Radius	Adopted	References
(1)	(2)	(3)	(4)
H II regions			
HK 16	0.84	8.28 ± 0.20	1
HK 42	0.90	8.43 ± 0.20	1
HK 69	0.10	$> 8.10^a$	1
HK 70	0.22	8.30 ± 0.20	1
Hodge 5	1.11	8.23 ± 0.20	2
Hodge 6	0.78	8.24 ± 0.20	2
Hodge 7	0.45	8.26 ± 0.20	1
Hodge 8	1.11	8.26 ± 0.15	3
Hodge 10 ^b	0.91	8.07 ± 0.08	3, 4
Hodge 12 ^c	0.08	7.9 ± 0.1	1
Hubble I	1.37	7.98 ± 0.09	1, 2, 3
Hubble II	1.02	8.27 ± 0.20	2
Hubble III	1.28	8.11 ± 0.20	1, 2, 3
Hubble V	1.03	8.14 ± 0.05	1, 2, 3, 5, 6, 7, 8, 9, 10, 11
Hubble X	1.20	8.01 ± 0.05	2, 3, 6, 7, 9, 10, 11
K α	1.00	8.00 ± 0.04	1, 4
K β	0.87	8.18 ± 0.07	1, 4
K γ	1.08	8.02 ± 0.04	4
KD 9	0.87	8.23 ± 0.20	1
KD 12 ^d	0.98	> 7.80	4
KD 13	1.16	8.26 ± 0.16	3
KD 20 ^d	0.21	> 7.93	1, 4
KD 21	1.06	8.31 ± 0.20	1
KD 22e	1.02	8.22 ± 0.20	1
KD 24	0.17	$> 8.13^a$	1
KD 25	0.40	8.37 ± 0.20	1
KD 28	1.90	8.22 ± 0.20	1
KD 28e	0.07	8.19 ± 0.05	1
Planetary nebulae			
S16	0.25	8.01 ± 0.16	12
S33	0.48	8.10 ± 0.08	12, 13
A-type supergiant stars			
CW 22	1.23	8.20 ± 0.10	14
CW 173	0.40	8.28 ± 0.17	15, 16
CW 185	0.29	8.44 ± 0.09	15, 16

NOTE. — Col. (1): Identifications - H II regions from Killen & Dufour (1982) and Hodge et al. (1988); planetary nebulae from Killen & Dufour (1982); A-type supergiant stars from Wilson (1992). Col. (2): Deprojected galactocentric radius, calculated using the parameters listed in Table 1. Cols. (3) and (4): Oxygen abundances and references, respectively.

REFERENCES. — (1) present work; (2) Pagel et al. (1980); (3) Talent (1980); (4) Chandar et al. (2000); (5) Peimbert & Spinrad (1970); (6) Smith (1975); (7) Lequeux et al. (1979); (8) Skillman et al. (1989); (9) Hidalgo-Gómez et al. (2001); (10) Miller (1996); (11) Peimbert et al. (2005); (12) Richer & McCall (1995); (13) Dufour & Talent (1980); (14) Lee et al. (2003d); (15) Venn et al. (2001); (16) Venn & Miller (2002).

^aLower limits due to zero and noisy detection of [O III] $\lambda 5007$ in HK 69 and KD 24, respectively.

^bAlso known as Hubble IV, KD 18.

^cSupernova remnant.

^dKD 12 and KD 20 identified as C9 and C10, respectively, in Chandar et al. (2000).

TABLE 8
LINEAR LEAST-SQUARES FITS TO VARIOUS SUBSETS OF OXYGEN ABUNDANCE DATA.

Data subset	Linear	Rms about
(1)	Least-Squares Fit	fit (dex)
	(2)	(3)
(a): All nebulae in present work	$\mathcal{Y} = (8.21 \pm 0.07) + (-0.02 \pm 0.07)R$	0.14
(b): A-type supergiants + set (a)	$\mathcal{Y} = (8.25 \pm 0.06) + (-0.05 \pm 0.07)R$	0.14
(c): H II s with [O III] $\lambda 4363$: present work	$\mathcal{Y} = (8.23 \pm 0.06) + (-0.14 \pm 0.07)R$	0.06
(d): A-type supergiants	$\mathcal{Y} = (8.43 \pm 0.06) + (-0.19 \pm 0.08)R$	0.06
(e): H II s with [O III] $\lambda 4363$: set (c) + liter.	$\mathcal{Y} = (8.23 \pm 0.05) + (-0.16 \pm 0.05)R$	0.05
(f): Sets (d) + (e)	$\mathcal{Y} = (8.34 \pm 0.07) + (-0.24 \pm 0.07)R$	0.09

NOTE. — \mathcal{Y} represents the oxygen abundance, $12+\log(\text{O}/\text{H})$, and R represents the linear galactocentric radius in kpc. Dataset a is the set of measurements for all nebulae in the present work. Dataset b combines the previous dataset with measurements for A-type supergiants. Dataset c is the set of [O III] $\lambda 4363$ measurements for the five H II regions in the present work. Dataset d is a fit only to the A-type supergiants. Dataset e is the set of [O III] $\lambda 4363$ measurements for the five H II regions in this work and three other [O III] $\lambda 4363$ detections from the literature (Chandar et al. 2000; Peimbert et al. 2005). We adopt oxygen abundances for all H II regions which were remeasured in the present work (e.g., Hubble V). Dataset f combines the previous dataset with measurements for A-type supergiants. The obtained linear least-squares fit to every dataset is shown as a solid line in the corresponding panel in Fig. 13.

This figure "f1.jpg" is available in "jpg" format from:

<http://arxiv.org/ps/astro-ph/0512428v1>

This figure "f2.jpg" is available in "jpg" format from:

<http://arxiv.org/ps/astro-ph/0512428v1>

This figure "f3.jpg" is available in "jpg" format from:

<http://arxiv.org/ps/astro-ph/0512428v1>

This figure "f4.jpg" is available in "jpg" format from:

<http://arxiv.org/ps/astro-ph/0512428v1>

This figure "f5.jpg" is available in "jpg" format from:

<http://arxiv.org/ps/astro-ph/0512428v1>

This figure "f6.jpg" is available in "jpg" format from:

<http://arxiv.org/ps/astro-ph/0512428v1>

This figure "f7.jpg" is available in "jpg" format from:

<http://arxiv.org/ps/astro-ph/0512428v1>

This figure "f9.jpg" is available in "jpg" format from:

<http://arxiv.org/ps/astro-ph/0512428v1>